NK026680 on T-cell function *in vitro* and the *in vivo* immunosuppressive effects of NK026680 alone or in combination with tacrolimus in a fully MHC-incompatible rat cardiac transplantation model.

2. Materials and methods

2.1. Animals

Male C57BL/6 (B6; H-2^b haplotype) and BALB/c (H-2^d) mice were purchased from Japan SLC (Shizuoka, Japan). Male Lewis ($RT1^l$ haplotype) and ACI ($RT1^{av1}$) rats were purchased from Kyudo (Fukuoka, Japan). Animals were maintained in a specific pathogen-free facility and used at 9–12 weeks of age. All experiments were approved by the Institutional Animal Care Committee and conducted under the Guidelines for the Care and Use of Laboratory Animals of Hokkaido University.

2.2. Reagents

NK026680 (molecular weight = 419 Da) [17] was provided by Nippon Kayaku Co., Ltd. The powder form of NK026680 was dissolved in 0.05% dimethylsulfoxide (Sigma-Aldrich; St. Louis, MO) for *in vitro* assays and suspended in 0.5% carboxymethylcellulose (CMC; Shin-Etsu Chemical Industry; Tokyo, Japan) for *in vivo* experiments due to its poor water solubility. Tacrolimus powder (20%: Asteras Pharmaceutical Co.; Osaka, Japan) was dissolved in distilled water. Anti-mouse CD3 (145-2C11), CD4 (RM4-5), CD25 (7D4), and CD28 (37.51) monoclonal antibodies (mAbs) and anti-human CD3 (HIT3a) and CD28 (CD28.2) mAbs were obtained from BD Biosciences (San Jose, CA). Anti-rat CD4 (W3/25) and CD8 (OX-8) antibodies (Abs) were obtained from AbD Serotec (Oxford, UK). Abs against phospho-p38 mitogen-activated protein kinase (MAPK) (Thr180/Tyr182), p38 MAPK, phospho-p44/p42 MAPK (extracellular signal-regulated kinase 1/2; ERK1/2) (Thr202/Tyr204), p44/p42 MAPK, phospho-stress-activated protein kinase (SAPK)/c-Jun NH2-terminal kinase (JNK), SAPK/JNK, and horseradish peroxidase-conjugated anti-rabbit IgG were obtained from Cell Signaling Technology (Beverly, MA).

2.3. Cell preparation and culture

Primary murine and rat leukocytes were isolated from spleens. After erythrocyte lysis with ACK buffer (Lonza, Walkersville, MD), T cells were enriched to greater than 90% purity by passing the cell suspension through a nylon-wool mesh column (R&D Systems, Minneapolis, MN). Human peripheral blood mononuclear cells (PBMCs) were obtained from the peripheral blood of healthy volunteers. After erythrocyte lysis, $CD4^+$ T cells were enriched to greater than 95% purity via a $CD4^+$ T-cell isolation kit and a magnetic cell separation system (Miltenyi Biotec, Auburn, CA). Complete RPMI 1640 media containing 2 mM L-glutamine, 100 U/ml penicillin, 100 μg/ml streptomycin, 10% fetal bovine serum, and 50 μM 2-mercaptoethanol were used for all cell cultures.

2.4. Proliferation assays

2.4.1. Mouse

For the mixed lymphocyte reaction (MLR), irradiated (30Gy, 137Cs) BALB/c mouse splenocytes (5×10^5 cells/well) were co-cultured with B6 mouse splenocytes (5×10^5 cells/well) for 3 days. Purified B6 mouse T cells (5×10^5 cells/well) were stimulated with 1 μg/ml anti-CD28 (αCD28) mAb and 1 μg/ml plate-bound anti-CD3 (αCD3) mAb for 2 days.

2.4.2. Rat

Irradiated ACI rat splenocytes (2×10^5 cells/well) were co-cultured with Lewis rat lymphocytes (2×10^5 cells/well) obtained from the cervical and auxiliary lymph nodes for 5 days. Purified Lewis rat T cells (2×10^5 cells/well) were stimulated with concanavalin A (Con A; 2 μg/ml; Sigma-Aldrich) for 3 days.

2.4.3. Human

Irradiated PBMCs (1×10^5 cells/well) were co-cultured with allogeneic PBMCs (1×10^5 cells/well) for 5 days. T cells (1×10^5 cells/well) were stimulated with 1 μg/ml αCD28 mAb and 1 μg/ml plate-bound αCD3 mAb for 3 days.

2.4.4. Proliferation assay

Cells were cultured in complete RPMI 1640 media at 37 °C and 5% CO_2 plus air. Cells were pulsed with ^{3}H-thymidine (1 μCi/well) 8 or 16 h before the analysis of thymidine incorporation with a β-counter (Perkin Elmer; Boston, MA).

2.5. Flow cytometry

Cells were stained with an isotype control or specific mAbs against CD4 and CD25 and then analyzed with a FACS Calibur flow cytometer and CellQuest software (BD Biosciences). For each analysis, 10,000 $CD4^+$ lymphocytes were acquired.

2.6. Cytokine measurement

IL-2 protein levels in culture supernatants were measured by enzyme-linked immunosorbent assay with a cytokine assay kit (R&D Systems). All measurements were performed in duplicate. The IFN-γ production of lymphocytes obtained from transplant recipients was examined by enzyme-linked immunospot assay as previously described [20].

2.7. Cell cycle analysis

Cell cycle analysis was performed using a Bromodeoxyuridine (BrdU) Flow Kit (BD Biosciences). Stimulated B6 mouse T cells were incubated with 10 μM BrdU for the final 30 min of culture, fixed, and permeabilized. DNA was digested by incubating cells with 300 μg/ml DNase at 37 °C for 60 min. Cells were stained with a fluorescein isothiocyanate-conjugated anti-BrdU Ab and 7-amino actinomycin D (7-AAD) prior to analysis by flow cytometry.

2.8. Nuclear protein extraction and quantification

Nuclear protein was harvested from 2×10^7 cells B6 mouse T cells according to the manufacturer's instructions (Nuclear Extract Kit; Activemotif, Carlsbad, CA). The levels of nuclear factor-kappa B (NF-κB), nuclear factor of activated T cells (NFAT), and activator protein-1 (AP-1) DNA binding activity were examined with the TransAM Kit (Activemotif) [21].

2.9. Immunoblotting

Cells were lysed with radioimmunoprecipitation assay buffer (50 mM Tris HCl, 150 mM NaCl, 1% NP40, 0.5% sodium deoxycholate, 0.1% sodium dodecyl sulfate, 1 mM ethylenediaminetetraacetic acid, and a protease inhibitor cocktail). Protein (30 μg) was resolved by 10% sodium dodecyl sulfate-polyacrylamide gel electrophoresis and transferred to nitrocellulose (Invitrogen, Carlsbad, CA). The membrane was blocked with 5% dry milk and 0.1% Tween (Sigma-Aldrich) in PBS, incubated with primary Ab, and then incubated with horseradish peroxidase-conjugated secondary Ab. Bands were detected by enhanced chemiluminescence.

2.10. Cardiac transplantation and treatment protocol

Intraabdominal heterotopic cardiac transplantation was performed as described by Ono and Lindsey [22]. The beating of the cardiac graft was monitored by daily palpation through the recipient's abdominal wall. Rejection was defined as the time of cessation of graft beating as confirmed by direct inspection and histological examination. Recipient animals were administered NK026680 (20, 30, or 40 mg/kg), tacrolimus (1.0 or 2.5 mg/kg), or control vehicle (0.5% CMC) orally from day 0 to day 13 ($n=6$ each).

2.11. Combination index (CI) calculation

According to the method by Chou and Talalay [23] and Stepkowski et al. [24], the interaction between two drugs was assessed by the CI analysis. The parameter of *fa* represents the fraction of systems that are affected (% inhibition) by the dose at D. For graft survival, 100% protection ($fa=1$) was defined as 50-day survival for heart allografts. A CI equal to 1 indicates additivity, less than 1 is synergism, and greater than 1 is antagonism.

2.12. Histology and immunohistochemistry

Cardiac grafts were excised at the time of animal death or sacrifice. Some of the tissue were fixed in 10% formalin, embedded in paraffin, and stained with hematoxylin and eosin (H&E). Graft samples were also embedded in an optimal cutting temperature compound, frozen in liquid nitrogen, and stored at −80 °C. Frozen sections were stained with anti-CD4 and anti-CD8 Abs by the avidin–biotin complex method [25]. Positive cells were counted in three different high power fields (magnification: ×400).

2.13. Statistical analysis

Graft survival time was plotted using the Kaplan–Meier method, and a log-rank test was applied for comparison between the groups. Other results were expressed as mean ± standard error of the mean (SEM). The Student *t*-test was used for the statistical analysis of paired comparisons, while analysis of variance with the Tukey–Kramer post hoc test was used for multiple comparisons. $P<0.05$ was considered statistically significant.

3. Results

3.1. NK026680 acts directly on T cells to suppress their proliferation in vitro

We began our study of NK026680 by investigating its effects on T lymphocytes. To determine if this compound exerted a suppressive effect on lymphocyte proliferation, a MLR assay was performed with murine leukocytes. The addition of NK026680 to culture medium suppressed the MLR in a dose-dependent manner starting at 10 ng/ml (Fig. 1A). The graph showed a 50% inhibitory concentration (IC50) of 50 ng/ml. Next, the effect of NK026680 on purified B6 mouse T cells stimulated with αCD3/αCD28 mAbs was assessed, and we found that NK026680-mediated inhibition of mAb-driven T-cell proliferation was dose-dependent with an IC50 value of 100 ng/ml (Fig. 1B). The suppressive effects of NK026680 on the MLR and T-cell proliferation were confirmed in rat (Fig. 1C and D) and human (Fig. 1E and F) cells. To eliminate NK026680 cytotoxicity as a source of these inhibitory effects, cellular viability was confirmed using a tetrazolium colorimetric assay. Cytotoxicity was not detected in mouse T cells treated with up to 500 ng/ml of NK026680 for 8 h: The viability of T cells after exposure to 500 ng/ml NK026680 showed 85.3 ± 7.1% of control treated with vehicle ($p=0.091$).

3.2. NK026680 inhibits CD25 upregulation, IL-2 production, and cell cycle progression in stimulated T cells

To further investigate the inhibitory properties of NK026680 on T-cell function, cellular activation, cytokine production, and cell cycle progression were examined in αCD3/αCD28-stimulated murine T cells. In the control $CD4^+$ T cells, cell surface expression of CD25 were upregulated after αCD3/αCD28 stimulation for 12 h. NK026680 suppressed CD25 expression in activated $CD4^+$ T cells at ≥50 ng/ml (Fig. 2A). Also, activated NK026680-treated T cells produced less IL-2 than activated control T cells by NK026680 treatment at ≥10 ng/ml (Fig. 2B). Analysis of cell cycle progression revealed that in the absence of NK026680, 42.5 ± 1.3% of the activated $CD4^+$ T cells transitioned through S-phase at 24 h. However, after NK026680 treatment, only 6.6 ± 0.9% of the activated $CD4^+$ T cells had entered S-phase at 24 h, and 91.2 ± 0.2% of the T cells were arrested in G0/G1 (Fig. 2C).

3.3. NK026680 regulates p38 MAPK phosphorylation and inhibits nuclear activation of p65, c-Fos, and c-Jun in activated T cells

To elucidate the molecular mechanisms of the suppressive effects of NK026680 on T cells, we examined its effect on the MAPK pathways that are critical in T-cell receptor (TCR) signaling following activation [26]. Immunoblotting demonstrated that NK026680 treatment significantly reduced p38 MAPK phosphorylation 30 min after αCD3/αCD28 stimulation of T cells. In contrast, the phosphorylation of ERK and JNK was not affected (Fig. 3A and B). We then examined the effect of NK026680 on downstream mediators of the MAPK pathways, including AP-1, NFAT and NF-κB, that play crucial roles in T-cell activation and subsequent IL-2 production [27,28]. The levels of NF-κB (p65 and p50), NFATc1, and AP-1 (c-Jun and c-Fos) within the nucleus increased shortly after stimulation in control T cells. NK026680 significantly suppressed the nuclear binding of p65, c-Fos and c-Jun, but not p50 and NFATc1 (Fig. 3C).

3.4. NK026680 alone or in combination with tacrolimus prolongs rat cardiac allograft survival

NK026680-mediated immunosuppression was examined in a rat heart transplantation model. Vehicle-treated control Lewis rats promptly rejected ACI rat cardiac allografts at a median survival time (MST) of 6 days. NK026680 at a dose of 20 mg/kg was insufficient for graft protection (MST; 6.5 days), but 30 mg/kg and 40 mg/kg doses of NK02680 significantly prolonged graft MST to 19 and 22.5 days, respectively (Table 1). A mild degree of diarrhea and a weight loss of less than 10% were observed in the group of NK026680 treatment by 40 mg/kg/day, but no severe adverse events leading to animal death were noted. Daily treatment with tacrolimus at 1.0 mg/kg and 2.5 mg/kg prolonged graft MST to 9 and 20.5 days, respectively. The combination therapy of 30 mg/kg of NK026680 and 1.0 or 2.5 mg/kg of tacrolimus prolonged graft MST to 28 or 33 days, respectively (Table 1). To assess the efficacy of combination therapy, the CI value was calculated according to the previous reports [23,24]. Each CI value was 0.904 and 0.987, indicating the additive or slight synergistic interaction between NK026680 and tacrolimus *in vivo*. No obvious augmentation of the adverse events leading cause of death was noted.

3.5. NK026680 combined with tacrolimus augments the regulation of alloimmune responses in vivo

To further understand how NK026680 treatment prevents allograft rejection *in vivo*, alloreactive lymphocytes and IFN-γ producing cells were evaluated at 4 and 10 days after transplantation (Fig. 4A). Lymphocytes isolated from the cervical and axillary lymph nodes of recipient rats were used as responder cells, while ACI rat splenocytes were used as the donor–antigen cells. Compared to lymphocytes from control animals, lymphocytes from rats treated with NK026680 showed reduced proliferation and had less IFN-γ spot-forming cells 4 days after donor–antigen stimulation. However, on day 10, the inhibitory effects of both NK026680 monotherapy and tacrolimus monotherapy were insufficient to control cellular alloreactivity. When a combination therapy that utilized NK026680 plus tacrolimus was utilized, the inhibitory effects of NK026680 were enhanced at days 4 and 10 (Fig. 4A). Finally, the ability of NK026680 to suppress cellular infiltration into the graft was evaluated by histopathology on day 4 (Fig. 4B and C). Without treatment, a considerable number of $CD4^+$ and $CD8^+$ cells infiltrated into the cardiac allograft by 4 days post-transplantation. In contrast, NK026680 treatment reduced infiltration of both T-cell populations into the graft. Moreover, the inhibitory effect of NK026680 was amplified by the addition of tacrolimus treatment, as co-administration prevented $CD4^+$ and $CD8^+$ cellular infiltration and allograft cardiomyocyte destruction at day 4 (Fig. 4B and C).

4. Discussion

In the current study, the triazolopyrimidine derivative NK026680 inhibited T-cell proliferation in an IL-2-dependent manner. Previous studies have shown a minimal inhibitory effect of NK026680 on αCD3/αCD28-mediated T-cell proliferation in humans [i.e., IC50 of 427 nM (179 ng/ml)] [17] as well as on Con A-induced T-cell proliferation in rats [100 nM (42 ng/ml)] [19]. However, our findings demonstrate that NK026680 inhibits proliferation of mouse, rat, and human T cells at a concentration of 50 ng/ml (Fig. 1). In addition to inhibiting proliferation, NK026680 reduced IL-2 production, downregulated CD25 (IL-2Rα) expression, and induced G0/G1-phase arrest (Fig. 2). We also confirmed by a tetrazolium colorimetric assay that the observed effects of NK026680 were not due to cytotoxicity.

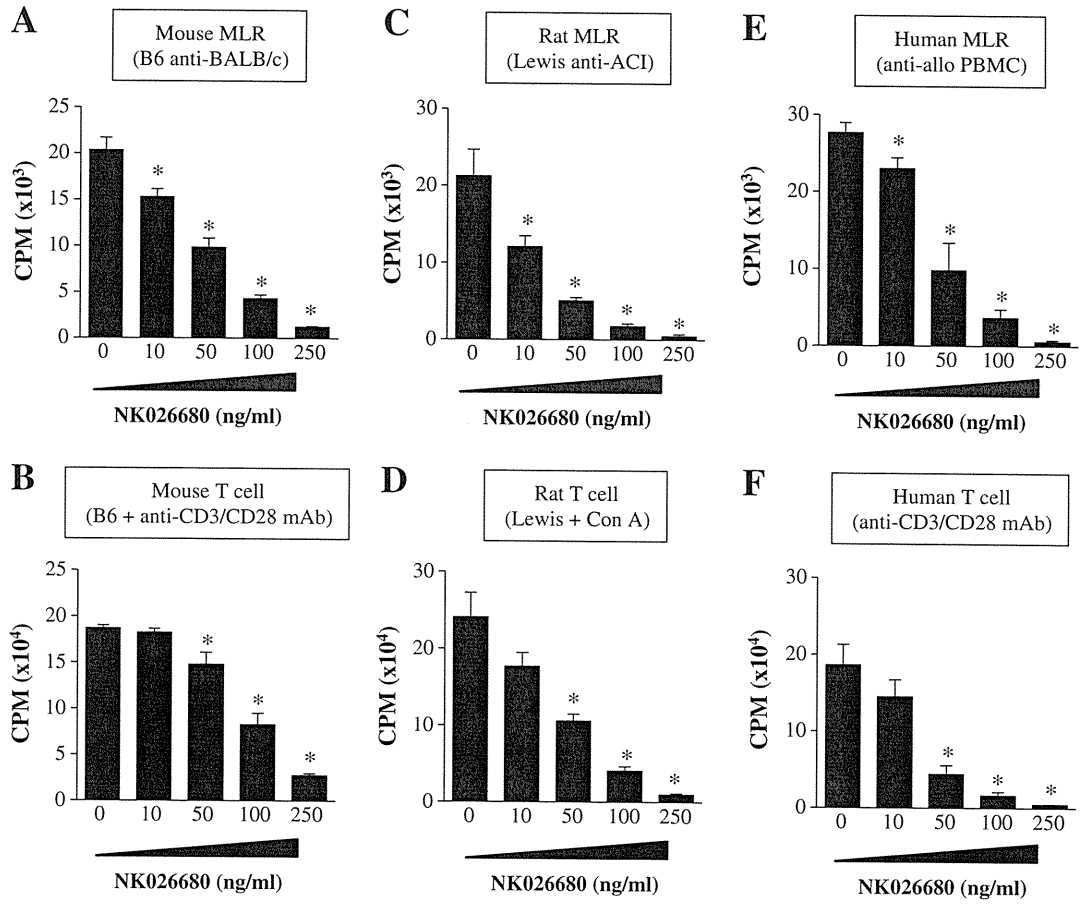

Fig. 1. NK026680 inhibits lymphocyte and T-cell proliferation in a dose-dependent manner. Lymphocytes and T cells isolated from mice, rats, and humans were stimulated with allogeneic antigen, monoclonal antibody (mAb), or mitogen with or without NK026680. Cells were pulsed with ^{3}H-thymidine at 8 or 16 h before cell harvest. Thymidine incorporation was analyzed at the indicated time points. (A) B6 mouse lymphocyte proliferation following 3-day stimulation with irradiated BALB/c mouse splenocytes. (B) B6 mouse T-cell proliferation following 2-day stimulation with αCD3/αCD28 mAbs. (C) Lewis rat lymphocyte proliferation following 5-day stimulation with irradiated ACI rat splenocytes. (D) Lewis rat T-cell proliferation following 3-day stimulation with Con A. (E) Human lymphocyte proliferation following 5-day stimulation with irradiated allogeneic PBMCs. (F) Human T-cell proliferation following 3-day stimulation with αCD3/αCD28 mAbs. Each bar represents the mean ± SEM of three independent experiments (*p<0.05 vs. control).

IL-2 plays an essential role in the process of T-cell activation. Soon after TCR activation and CD28 co-ligation, the various downstream mediators of the TCR signaling pathway such as MAPK [26] and transcriptional regulators including NFAT, NF-κB, and AP-1 [28] are activated. Subsequently, T cells produce and secrete IL-2, which induces synthesis of the IL-2 receptor. IL-2 signaling is involved in cell cycle progression from the G0/G1- to S-phase, leading to T-cell proliferation [29]. The activation of p38 MAPK itself can also regulate the nuclear activities of these transcription factors. Previous studies have shown that p38 MAPK activates NF-κB by phosphorylating inhibitor kappa B-α or mitogen- or stress-activated protein kinase-1 [30–32] and has both positive and negative effects on NFAT activation [33,34]. It has been suggested that p38 MAPK regulates AP-1 directly by phosphorylating activating transcription factor-2 and indirectly by inducing *c-fos* and *c-jun* gene expression [35]. In the present study, phosphorylation of p38 MAPK and the nuclear binding of c-Fos, p65, and to a lesser extent, c-Jun, were suppressed by NK026680 treatment (Fig. 3). These findings suggest that NK026680 regulates T-cell activation through inhibition of the p38 MAPK pathway, resulting in the suppression of AP-1 and NF-κB activation. This is in accord with a previous study in which a specific inhibitor of p38 MAPK, SB203580, inhibited IL-2 production by suppressing the nuclear localization of c-Jun and activating transcription factor-2 in activated mouse T cells [36]. Further investigation is necessary to determine if NK026680 acts specifically on p38 or if other mechanisms of action are involved. The AP-1 itself, in addition to the direct involvement in IL-2 production, also has an important ability to form complexes with the NFAT and NF-κB transcription factors: the proximal NFAT binding sites of the IL-2 promoter cooperatively bind both NFAT and AP-1, and likewise the CD28RE site of the IL-2 promoter is a cooperative binding site for NF-κB and AP-1 [37]. We consider that the cooperative interaction by inhibition of both p-65 and AP-1 results in such inhibitory effects on T-cell activation, although each inhibitory effect on these factors is not so powerful.

We have shown that NK026680 treatment prolongs cardiac allograft survival in a dose-dependent manner (Table 1). This *in vivo* effect parallels the suppression of the MLR, the expansion of donor-antigen reactive, IFN-γ-producing cells, and intragraft cellular infiltration (Fig. 4). A previous study by Hara et al. has demonstrated that NK026680 prolongs liver allograft survival in rats [19]. This *in vivo* study suggested that DCs modulated by NK026680 treatment were polarized toward a Th2 cytokine profile, which resulted in an attenuation of T-cell responses. In fact, previous *in vitro* experiments have indicated that NK026680 inhibited IL-12p70 production and CD86 expression in activated DCs at 40 to 50 nM (16.8 to 21 ng/ml) [17,19], a concentration far below the concentration of NK026680 shown to effectively inhibit T cells in this study. On the other hand, in rat treated orally with a single dose of 20 mg/kg and 50 mg/kg, the maximal plasma concentration of

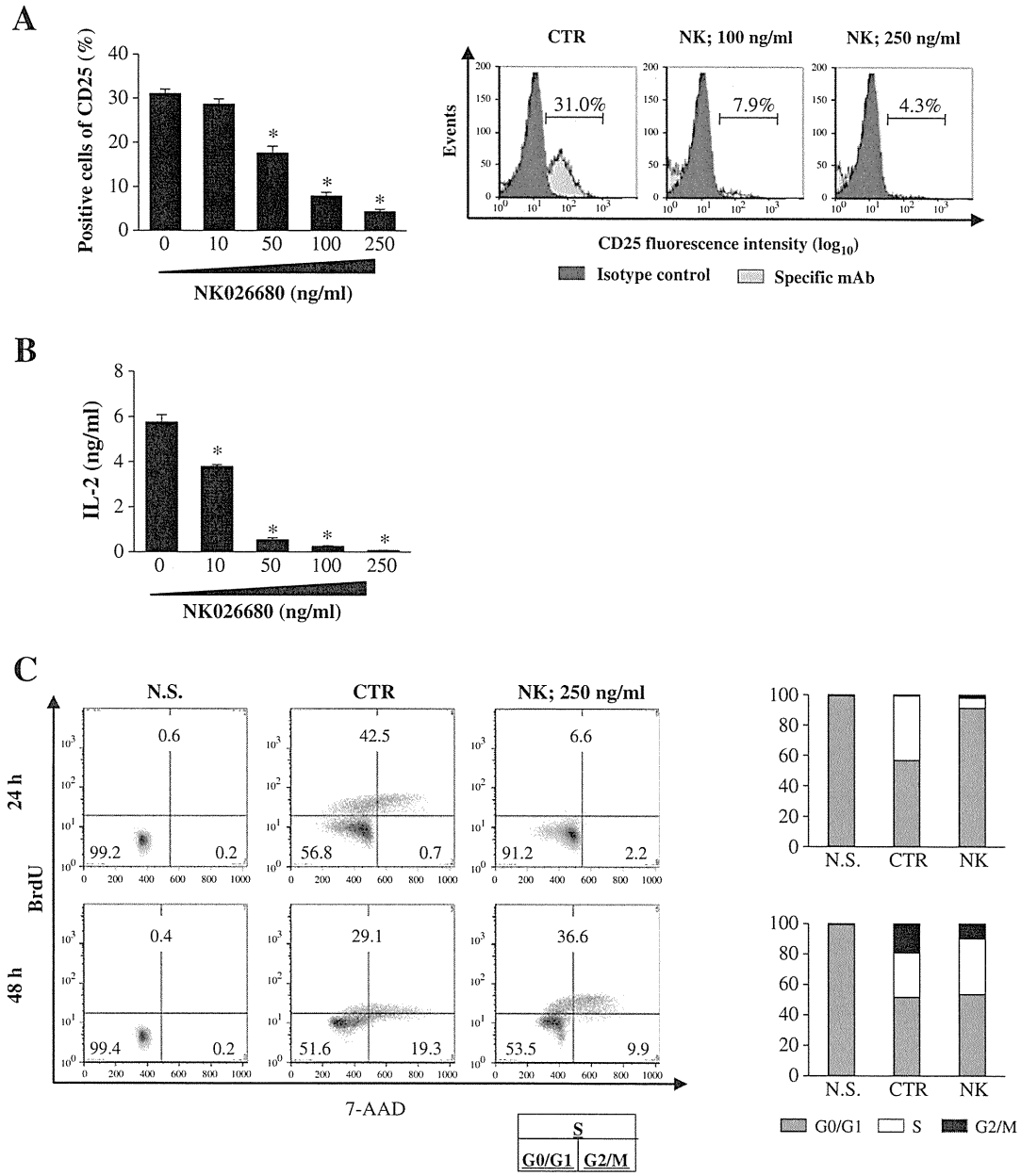

Fig. 2. NK026680 suppresses CD25 upregulation, IL-2 production, and cell cycle progression in naïve B6 mouse T cells. Naïve B6 mouse T cells were cultured with αCD3/αCD28 mAbs in the presence of vehicle alone (CTR) or NK026680 (NK; 100 or 250 ng/ml). (A) Cell surface CD25 expression of T cells following 12 h stimulation. T cells were harvested, stained with specific mAbs, and analyzed by flow cytometry after gating on 10,000 $CD4^+$ events. Each bar represents the mean ± SEM of three independent experiments (*left*, $^*p \leq 0.05$ vs. CTR). Representative histograms of three independent experiments with similar results are shown (*right*). (B) IL-2 production by T cells after 48 h mAb stimulation. Protein levels in culture supernatants were measured by enzyme-linked immunosorbent assay. Each bar represents the mean ± SEM of three independent experiments ($^*p < 0.05$ vs. CTR). (C) Cell cycle progression in T cells stimulated with mAb for 24 or 48 h. Cells were pulsed with BrdU 30 min before cell harvest, stained intracellularly with 7-AAD, and analyzed by flow cytometry. The results shown are representative of three independent experiments with similar results (*left*). Each bar represents the mean of three independent experiments (*right*; $^*p < 0.05$ vs. CTR; N.S., no stimulation).

NK026680 was over 500 ng/ml and 800 ng/ml, and the concentration 4 h after administration was approximately 125 ng/ml and 240 ng/ml, respectively (Shinichi Matsumoto et. al., unpublished data). These data suggest that, in addition to the effects on DCs, impairment of the T-cell response resulting from the suppression of IL-2, which we demonstrated in our *in vitro* study, contributes to the prolongation of allograft survival.

NK026680 treatment led to prolonged graft survival, but the administration of this agent alone was not sufficient to prevent acute rejection after drug cessation. However, NK026680 treatment in combination with tacrolimus further improved graft survival (Table 1). In regard to drug interactions, the concentration of each compound in the blood was unaffected by their combined administration, as there was little difference in the serum NK026680 trough levels (NK026680 alone; 1.9 ± 1.8 vs. combination; 1.2 ± 2.1 ng/ml) and the blood tacrolimus levels (tacrolimus alone; 0.8 ± 0.6 vs. combination; 0.5 ± 0.1 ng/ml) between cardiac recipient rats 10 days after transplantation.

Regarding the drug-related toxicity of NK026680, previous studies have revealed that treatment with NK026680 did not show any

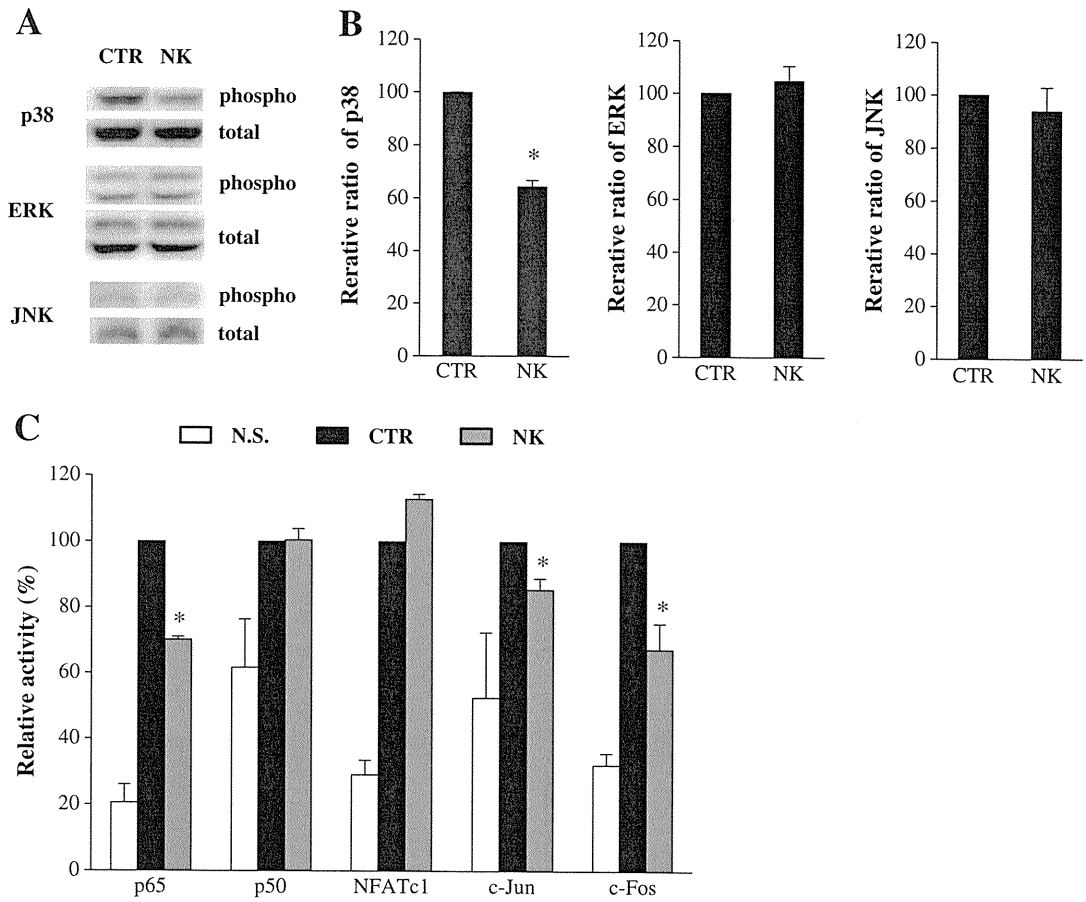

Fig. 3. NK026680 reduces p38 MAPK phosphorylation and suppresses the nuclear activity of p65 and AP-1 in mAb-stimulated T cells. Naïve B6 mouse T cells were stimulated with αCD3/αCD28 mAbs in the absence (CTR) or presence of NK026680 (NK; 250 ng/ml). (A and B) MAPK phosphorylation in T cells stimulated for 30 min. Immunoblotting with Abs against phospho- or total p38 MAPK (p38), ERK1/2 (ERK), and SAPK/JNK (JNK) was performed. Bands were visualized by chemiluminescence. (A) A representative immunoblot of three independent experiments. (B) Densitometry and the relative ratio of phospho- to total p38, ERK, and JNK. Each bar represents the mean ± SEM of three independent experiments (*$p<0.05$ vs. CTR). (C) DNA binding activity of nuclear NF-κB, NFATc1, and AP-1 in T cells stimulated for 2 h. Nuclear extracts were prepared from T cells, and DNA binding activity was quantified using the TransAM kit. The relative activity of nuclear p65, p50, NFATc1, c-Jun, and c-Fos is shown. Each bar represents the mean ± SEM of three independent experiments (*$p<0.05$ vs. CTR; N.S., no stimulation).

genotoxicity or histopathological organ damage in mice [17], and that a long-term administration of NK026680 did not induce severe toxic effects in rats [18]. In our current study, no apparent adverse events leading to animal death occurred by NK026680 treatment, while a mild degree of diarrhea and weight loss were observed when administered at a dose of 40 mg/kg/day. Based on previous reports and our data, oral administration of NK026680 up to a daily dose of 40 mg/kg seems to be well tolerable for immunosuppression *in vivo*. However,

Table 1
Efficacy of NK026680 alone or in combination with tacrolimus in ACI-to-LEW rat heart transplantation.

Group	Drug (mg/kg/day)[a]		Graft survival (days)	Median (days)	$p^b<0.05$	*fa*	CI[c]
	NK026680	Tacrolimus					
1	–	–	6, 6, 6, 6, 7, 7	6		–	
2	20	–	6, 6, 6, 7, 7, 7	6.5		0.01	
3	30	–	18, 18, 19, 19, 19, 22	19	vs. group 1,2	0.24	
4	40	–	20, 21, 21, 24, 24, 32	22.5	vs. group 1,2	0.31	
5	–	1.0	8, 8, 9, 9, 9, 10	9	vs. group 1	0.06	
6	–	2.5	20, 20, 20, 21, 21, 22	20.5	vs. group 1,5	0.29	
7	–	5.0	21, 23, 23, 24, 24, 25	23.5	vs. group 1,5	0.34	
8	30	1.0	24, 24, 28, 28, 29, 30	28	vs. group 1,3,5	0.44	0.904
9	30	2.5	26, 29, 33, 33, 34, 36	33	vs. group 1,3,6	0.54	0.987

[a] Drug was given orally to cardiac recipient animal for 14 days starting from the day of grafting. As a vehicle control, animals in the group 1 were administered 0.5% CMC only.
[b] A *p*-value was calculated by a log-rank test.
[c] CI (Combination index) values were calculated as described in Materials and methods.

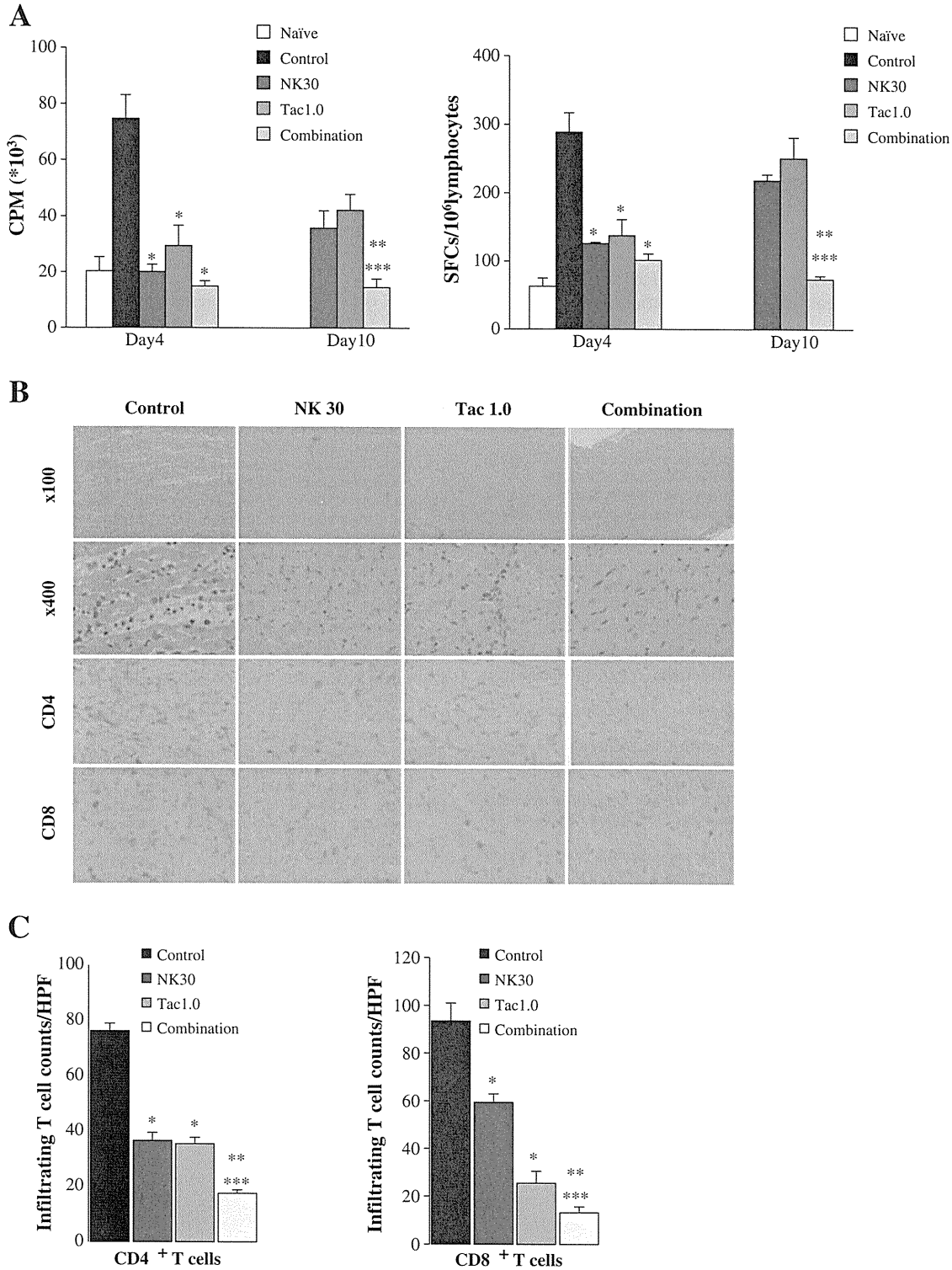

Fig. 4. NK026680 plus tacrolimus suppresses alloimmune responses and intragraft cellular infiltration. (A) Axillary and cervical lymphocytes obtained from cardiac recipients were co-cultured with irradiated ACI splenocytes at 4 and 10 days after transplantation. ^{3}H-thymidine uptake of alloreactive lymphocyte proliferation after 96 h of co-culture (*left*) and the number of alloreactive IFN-γ-producing cells as measured by enzyme-linked immunospot assay after 24 h of co-culture (*right*) are shown. Each bar represents the mean ± SEM of four independent experiments (*$p<0.05$ vs. control, **$p<0.05$ vs. NK30, ***$p<0.05$ vs. Tac1.0; SFCs, spot-forming cells). (B) Histology of cardiac grafts following transplantation. Cardiac allografts were stained with H&E (original magnification: ×100 or ×400), anti-CD4 (×400), and anti-CD8 Abs (×400). Representative photographs of four independent grafts on day 4 are shown. (C) The number of $CD4^+$ (*left*) and $CD8^+$ (*right*) cells in graft sections were counted in three different high power fields (HPFs) and quantified. Each bar represents the mean ± SEM of four independent experiments (*$p<0.05$ vs. control, **$p<0.05$ vs. NK30, ***$p<0.05$ vs. Tac1.0; NK30, NK026680 treatment at 30 mg/kg; Tac1.0, tacrolimus treatment at 1.0 mg/kg; combination, both NK30 and Tac1.0 treatment).

more detailed studies are warranted in the future to confirm the toxicity and pharmacologic interaction of NK026680 when used alone or in conjunction with other immunosuppressants including tacrolimus.

We conclude that NK026680 inhibits the activation of T cells and prolongs cardiac allograft survival in rats. NK026680 is a potential therapeutic candidate for immunosuppression following organ

transplantation both alone and in combination with tacrolimus or another conventional calcineurin inhibitor.

Disclosure statement

This study was supported in part by funding from the Nippon Kayaku Co., Ltd, Yutohkai, and Grant-in-Aid for Scientific Research from the Japan Society for the Promotion of Science, Japan.

Acknowledgements

We thank Dr. K. Saiga (Nippon Kayaku Co., Ltd) for providing us with NK026680 and for measuring its concentration in blood.

References

[1] Dunn CJ, Wagstaff AJ, Perry CM, Plosker GL, Goa KL. Cyclosporin: an updated review of the pharmacokinetic properties, clinical efficacy and tolerability of a microemulsion-based formulation (neoral)1 in organ transplantation. Drugs 2001;61(13):1957–2016.
[2] Scott LJ, McKeage K, Keam SJ, Plosker GL. Tacrolimus: a further update of its use in the management of organ transplantation. Drugs 2003;63(12):1247–97.
[3] Flechner SM, Kobashigawa J, Klintmalm G. Calcineurin inhibitor-sparing regimens in solid organ transplantation: focus on improving renal function and nephrotoxicity. Clin Transplant 2008;22(1):1–15.
[4] Ekberg H, Bernasconi C, Tedesco-Silva H, Vitko S, Hugo C, Demirbas A, et al. Calcineurin inhibitor minimization in the Symphony study: observational results 3 years after transplantation. Am J Transplant 2009;9(8):1876–85.
[5] Moore J, Middleton L, Cockwell P, Adu D, Ball S, Little MA, et al. Calcineurin inhibitor sparing with mycophenolate in kidney transplantation: a systematic review and meta-analysis. Transplantation 2009;87(4):591–605.
[6] Farkas SA, Schnitzbauer AA, Kirchner G, Obed A, Banas B, Schlitt HJ. Calcineurin inhibitor minimization protocols in liver transplantation. Transpl Int 2009;22(1):49–60.
[7] Zuckermann AO, Aliabadi AZ. Calcineurin-inhibitor minimization protocols in heart transplantation. Transpl Int 2009;22(1):78–89.
[8] Gocer AI, Ildan F, Tuna M, Polat S, Tamer L, Erman T, et al. Effects of trapidil on ATPase, lipid peroxidation, and correlation with ultrastructure in experimental spinal cord injury. Neurosurg Rev 2001;24(2–3):136–42.
[9] Bagdatoglu C, Saray A, Surucu HS, Ozturk H, Tamer L. Effect of trapidil in ischemia/reperfusion injury of peripheral nerves. Neurosurgery 2002;51(1):212–9 discussion 9–20.
[10] Colak T, Polat A, Bagdatoglu O, Kanik A, Turkmenoglu O, Aydin S. Effect of trapidil in ischemia/reperfusion injury on rat small intestine. J Invest Surg 2003;16(3):167–76.
[11] Somuncu S, Cakmak M, Erdogan S, Caglayan O, Akman H, Kaya M. Protective effects of trapidil in ischemia–reperfusion injury due to testicular torsion and detorsion: an experimental study. Int J Urol 2006;13(5):601–5.
[12] Avlan D, Tamer L, Ayaz L, Polat A, Ozturk C, Ozturhan H, et al. Effects of trapidil on renal ischemia–reperfusion injury. J Pediatr Surg 2006;41(10):1686–93.
[13] Maresta A, Balducelli M, Cantini L, Casari A, Chioin R, Fabbri M, et al. Trapidil (triazolopyrimidine), a platelet-derived growth factor antagonist, reduces restenosis after percutaneous transluminal coronary angioplasty. Results of the randomized, double-blind STARC study. Studio Trapidil versus Aspirin nella Restenosi Coronarica. Circulation 1994;90(6):2710–5.
[14] Galassi AR, Tamburino C, Nicosia A, Russo G, Grassi R, Monaco A, et al. A randomized comparison of trapidil (triazolopyrimidine), a platelet-derived growth factor antagonist, versus aspirin in prevention of angiographic restenosis after coronary artery Palmaz–Schatz stent implantation. Catheter Cardiovasc Interv 1999;46(2):162–8.
[15] Zhou L, Ismaili J, Stordeur P, Thielemans K, Goldman M, Pradier O. Inhibition of the CD40 pathway of monocyte activation by triazolopyrimidine. Clin Immunol 1999;93(3):232–8.
[16] Zhou L, Schandene L, Mordvinov VA, Chatelain P, Pradier O, Goldman M, et al. Trapidil inhibits monocyte CD40 expression by preventing IFN-gamma-induced STAT1 S727 phosphorylation. Int Immunopharmacol 2004;4(7):863–71.
[17] Saiga K, Toyoda E, Tokunaka K, Masuda A, Matsumoto S, Mashiba H, et al. NK026680, a novel compound suppressive of dendritic cell function, ameliorates mortality in acute lethal graft-versus-host reaction in mice. Bone Marrow Transplant 2006;37(3):317–23.
[18] Saiga K, Tokunaka K, Ichimura E, Toyoda E, Abe F, Yoshida M, et al. NK026680, a novel suppressant of dendritic cell function, prevents the development of rapidly progressive glomerulonephritis and perinuclear antineutrophil cytoplasmic antibody in SCG/Kj mice. Arthritis Rheum 2006;54(11):3707–15.
[19] Hara Y, Funeshima-Fuji N, Fujino M, Tokunaka K, Abe F, Sato Y, et al. A novel chemical compound, NK026680, targets dendritic cells to prolong recipient survival after rat liver grafting. Transplantation 2007;84(3):407–14.
[20] Ueki S, Yamashita K, Aoyagi T, Haga S, Suzuki T, Itoh T, et al. Control of allograft rejection by applying a novel nuclear factor-kappaB inhibitor, dehydroxymethylepoxyquinomicin. Transplantation 2006;82(12):1720–7.
[21] Renard P, Ernest I, Houbion A, Art M, Le Calvez H, Raes M, et al. Development of a sensitive multi-well colorimetric assay for active NFkappaB. Nucleic Acids Res 2001;29(4):E21.
[22] Ono K, Lindsey ES. Improved technique of heart transplantation in rats. J Thorac Cardiovasc Surg 1969;57(2):225–9.
[23] Chou TC, Talalay P. Quantitative analysis of dose–effect relationships: the combined effects of multiple drugs or enzyme inhibitors. Adv Enzyme Regul 1984;22:27–55.
[24] Stepkowski SM, Tian L, Napoli KL, Ghobrial R, Wang ME, Chou TC, et al. Synergistic mechanisms by which sirolimus and cyclosporin inhibit rat heart and kidney allograft rejection. Clin Exp Immunol 1997;108(1):63–8.
[25] Nomura M, Yamashita K, Murakami M, Takehara M, Echizenya H, Sunahara M, et al. Induction of donor-specific tolerance by adenovirus-mediated CD40lg gene therapy in rat liver transplantation. Transplantation 2002;73(9):1403–10.
[26] Ashwell JD. The many paths to p38 mitogen-activated protein kinase activation in the immune system. Nat Rev Immunol 2006;6(7):532–40.
[27] Jain J, Loh C, Rao A. Transcriptional regulation of the IL-2 gene. Curr Opin Immunol 1995;7(3):333–42.
[28] Huang Y, Wange RL. T cell receptor signaling: beyond complex complexes. J Biol Chem 2004;279(28):28827–30.
[29] Crabtree GR, Clipstone NA. Signal transmission between the plasma membrane and nucleus of T lymphocytes. Annu Rev Biochem 1994;63:1045–83.
[30] Vermeulen L, De Wilde G, Van Damme P, Vanden Berghe W, Haegeman G. Transcriptional activation of the NF-kappaB p65 subunit by mitogen- and stress-activated protein kinase-1 (MSK1). EMBO J 2003;22(6):1313–24.
[31] Huang C, Chen N, Ma WY, Dong Z. Vanadium induces AP-1- and NFkappaB-dependent transcription activity. Int J Oncol 1998;13(4):711–5.
[32] Zechner D, Craig R, Hanford DS, McDonough PM, Sabbadini RA, Glembotski CC. MKK6 activates myocardial cell NF-kappaB and inhibits apoptosis in a p38 mitogen-activated protein kinase-dependent manner. J Biol Chem 1998;273(14):8232–9.
[33] Wu CC, Hsu SC, Shih HM, Lai MZ. Nuclear factor of activated T cells c is a target of p38 mitogen-activated protein kinase in T cells. Mol Cell Biol 2003;23(18):6442–54.
[34] Gomez del Arco P, Martinez-Martinez S, Maldonado JL, Ortega-Perez I, Redondo JM. A role for the p38 MAP kinase pathway in the nuclear shuttling of NFATp. J Biol Chem 2000;275(18):13872–8.
[35] Chen Z, Gibson TB, Robinson F, Silvestro L, Pearson G, Xu B, et al. MAP kinases. Chem Rev 2001;101(8):2449–76.
[36] Zhang J, Salojin KV, Gao JX, Cameron MJ, Bergerot I, Delovitch TL. p38 mitogen-activated protein kinase mediates signal integration of TCR/CD28 costimulation in primary murine T cells. J Immunol 1999;162(7):3819–29.
[37] Foletta VC, Segal DH, Cohen DR. Transcriptional regulation in the immune system: all roads lead to AP-1. J Leukoc Biol 1998;63(2):139–52.

Co-Expression of Mesothelin and CA125 Correlates With Unfavorable Patient Outcome in Pancreatic Ductal Adenocarcinoma

Takahiro Einama, MD, Hirofumi Kamachi, MD,* Hiroshi Nishihara, MD,† Shigenori Homma, MD,* Hiromi Kanno, MD,‡ Kenta Takahashi, MD,‡ Ayami Sasaki, MD,* Munenori Tahara, MD,* Kuniaki Okada, MD,§ Shunji Muraoka, MD,|| Toshiya Kamiyama, MD,* Yoshihiro Matsuno, MD,¶ Michitaka Ozaki, MD,# and Satoru Todo, MD**

Objectives: Recent studies have shown that the high affinity of mesothelin-CA125 interaction might cause intracavitary tumor metastasis. We examined the clinicopathologic significance and prognostic implication of mesothelin and CA125 expression in pancreatic ductal adenocarcinoma.

Methods: Tissue samples from 66 pancreatic ductal adenocarcinomas were immunohistochemically examined. Proportion and intensity of constituent tumor cells with mesothelin and CA125 expression were analyzed and classified as high-level expression, defined as expression by more than 50% of tumor cells and/or moderate to strong staining, or low-level expression otherwise.

Results: A high level of mesothelin was correlated with a higher histological grade ($P = 0.049$) and the level of blood vessel permeation ($P = 0.0006$), whereas a high level of CA125 expression was correlated with a higher recurrence rate ($P = 0.015$). The expression of mesothelin was strongly correlated with that of CA125 ($P = 0.0041$). Co-expression of mesothelin and CA125 were associated with an unfavorable patient outcome ($P = 0.0062$).

Conclusions: This is the first report showing that co-expression of mesothelin and CA125 were in pancreatic ductal adenocarcinoma, and such co-expression is associated with a poor prognosis. Our finding suggests that co-expression of these two factors plays a significant role in the acquisition of aggressive clinical behavior.

Key Words: mesothelin, CA125, co-expression of mesothelin and CA125, pancreatic ductal adenocarcinoma

(*Pancreas* 2011;40: 1276–1282)

Pancreatic cancer is the fourth leading cause of cancer-related death in the United States.[1] Despite recent advances in diagnostic and therapeutic techniques, pancreatic cancer remains one of the most lethal malignancies. The 5-year survival rate of patients with primary pancreatic cancer after complete resection does not reach 15%,[2] whereas the overall 5-year survival rate in patients with inoperable pancreatic cancer is desperately low, ranging from 0.4% to 4%.[3,4] Therefore, a new predictive marker of malignant potential and prognosis and treatment for these patients is required.

Mesothelin is a 40-kDa cell surface glycoprotein and is expressed on normal mesothelial cells lining the pleura, pericardium, and peritoneum.[5,6] Moreover, mesothelin has been shown to be overexpressed in several cancer types, including mesothelioma, ovarian cancer, and pancreatic cancer.[7–10] The biological functions of mesothelin are not clearly understood, although recent studies have suggested that overexpression of mesothelin increases cell proliferation and migration.[11] In ovarian cancers, diffuse mesothelin staining was correlated with prolonged survival in patients with advanced-stage disease.[12] Another report indicated that a higher mesothelin expression is associated with chemoresistance and shorter patient survival.[13] In pancreatic cancer, mesothelin was immunohistochemically expressed in all cases but absent in normal pancreas and in chronic pancreatitis.[7,14,15]

CA125 is a cell surface glycoprotein that is present on normal mesothelial cells lining the body cavities.[16,17] Increased cell surface expression of CA125 is seen in tumors such as ovarian cancer and mesothelioma as well as certain other cancers.[16,18–20] It also sheds into the blood circulation. Serum CA125 is commonly measured to monitor disease progression in ovarian cancer patients and is also elevated in mesothelioma as well as in certain benign conditions.[21–23] The gene encoding the peptide moiety of CA125 has been cloned and termed MUC16 because it shares characteristics associated with mucin proteins.[24,25]

Mesothelin could be one of the binding partners for CA125.[26–28] In fact, heterotypic adhesion through the high-affinity interaction of mesothelin-CA125 could facilitate peritoneal metastasis from ovarian cancer.[26,28] To date, however, there have not been any studies regarding the significance of mesothelin and CA125 expression in pancreatic ductal adenocarcinoma. Therefore, we investigated the status of mesothelin and CA125 expressions in pancreatic ductal adenocarcinoma by immunohistochemistry and analyzed the relationship between mesothelin-CA125 expressions and clinicopathologic parameters, including patient relapse-free survival (RFS) and overall survival (OS).

MATERIALS AND METHODS

Patients Demographics and Tumor Specimens

This study was performed with the approval of the internal review board on ethical issues of Hokkaido University Hospital, Sapporo, Japan. The subjects of this study were 66 patients who underwent surgery with curative intent for primary pancreatic ductal adenocarcinoma between January 2000 and December

From the Departments of *General Surgery and †Translational Pathology, Hokkaido University Graduate School of Medicine; ‡Department of Pathology, Laboratory of Cancer Research, Hokkaido University School of Medicine; Departments of §Surgery and ||Pathology, JA Sapporo Kosei Hospital; ¶Department of Surgical Pathology, Hokkaido University Hospital; and #Department of Molecular Surgery, Hokkaido University School of Medicine, Sapporo, Japan.

Received for publication September 21, 2010; accepted April 20, 2011.

Reprints: Takahiro Einama, MD, Department of General Surgery, Hokkaido University Graduate School of Medicine, Kita-Ku, Kita 14, Nishi 7, Sapporo 060-8638, Japan (e-mail: titiuehahaue@hotmail.com).

This work was supported in part by a grant-in-aid from the foundation for the Department of General Surgery, Hokkaido University, Alumni Association.

The authors declare no conflict of interest.

2006 at the Department of General Surgery, Hokkaido University Graduate School of Medicine, and JA Sapporo Kosei Hospital (both in Sapporo, Japan). The clinicopathologic characteristics of these cases are summarized in Table 1.

The mean patient age was 64.7 (± 2.3 standard deviation [SD]) years. Thirty-six patients (54.5%) were men, and the remaining 30 (45.5%) were women. The location of the tumor was the pancreatic head in 44 (66.7%) patients and the body or/and tail in 22 (33.3%). Tumor stages comprising T, N, M factors; clinical stage; histological grade; and residual tumor were assigned according to the TNM classification of the Union for International Cancer Control.[29] Lymphatic permeation and blood vessel invasion were evaluated as either positive or negative. The median follow-up period for surviving patients was 66.1 months (range, 38.3–92.7 months).

Histologically, all 66 patients had invasive ductal adenocarcinoma of the pancreas, which was histological grade 1 (well differentiated) in 13 cases, 2 (moderately differentiated) in 42 cases, and 3 (poorly differentiated) in 11 cases, and were included.

Formalin-fixed paraffin-embedded tissue blocks were prepared from the patient's tumor specimens, and sections were cut and stained with hematoxylin-eosin (HE) for routine histopathologic examination. Pancreatic ductal adenocarcinoma was diagnosed in all specimens. A representative tissue block was selected from each case to perform immunohistochemical studies.

TABLE 1. Clinicopathologic Characteristics of 66 Patients With Pancreatic Ductal Adenocarcinoma in This Study

Parameter	No. Cases
Age, y	
<60	19
≧60	47
Mean (± SD)	64.7 (± 2.3)
Sex	
Male	36
Female	30
Location	
Pancreatic head	44
Pancreatic body or/and tail	22
T factor	
T1	9
T2	9
T3	47
T4	1
N factor	
N0	21
N1	45
M factor	
M0	59
M1	7
Stage	
IA	6
IB	4
IIA	12
IIB	36
III	1
IV	7
Residual tumor	
R0	44
R1	22

SD indicates standard deviation.

Immunohistochemistry

Four-micrometer-thick sections were mounted on charged glass slides, deparaffinized, and rehydrated through a graded ethanol series. For antigen retrieval, Dako Target Retrieval Solution pH 9.0 (catalog no. S2368) was used, and the slides were boiled in a pressure cooker (Pascal Pressure Cooker, model S2800; Dako Cytomation, Glostrup, Denmark) to a temperature of 125°C for 3 minutes. The sections were treated with 0.3% hydrogen peroxidase for 5 minutes to quench endogenous peroxidase activity. Subsequently, the slides were incubated with a 1:50 dilution of a mouse monoclonal antibody to mesothelin (clone 5B2 diluted 1:50; Novocastra, Newcastle Upon Tyne, UK) and to CA125 (clone M11 diluted 1:50; Dako, Kyoto, Japan) at room temperature for 30 minutes and then reacted with a dextran polymer reagent combined with secondary antibodies and peroxidase (Envision/HRP; Dako Cytomation) for 30 minutes at room temperature. Specific antigen-antibody reactions were visualized with 0.2% diaminobenzine tetrahydrochloride and hydrogen peroxide. Slides were counterstained with hematoxylin for 10 minutes, then rinsed gently in reagent quality water.

Immunohistochemical Evaluation

All assessments were made on the tumor region of the specimen (×200). Each slide was evaluated independently by 3 pathologists (T.E., H.K., K.T.), who did not know the clinical outcomes.

Immunostaining for mesothelin and CA125 was evaluated for both the proportion and staining intensity of tumor cells in each case. The levels of mesothelin and CA125 expression were assessed according to the percentage of cells showing each expression as follows: 1% to 10%, 10% to 50%, and greater than 50%.

Immunostaining for mesothelin and that for CA125 were each evaluated using the following scoring system: If incomplete membrane staining was observed and/or if faint or barely perceptible cytoplasmic staining was detected in the tumor cells, a score of 1+ was assigned. A score of 2+ was assigned if the entire circumference of the cell membrane was stained and/or if cytoplasmic staining demonstrated moderate to strong staining. Cytoplasmic granular staining was also scored as 2+ (Fig. 1). High-level expression was defined as greater than 50% of tumor cells irrespectively of intensity of immunoreactions and/or moderate to strong staining irrespectively of proportion of immunoreactive cells, and low-level expression was defined as weak immunoreactions in 50% or less of cancer cells or the absence of immunoreaction. We defined the co-expression as positive in patient groups with a high level of mesothelin expression and a high level of CA125 expression and the co-expression as negative in patient groups with a high-level mesothelin expression and a low-level CA125 expression, those with a high-level CA125 expression and a low-level mesothelin expression, and those with a low-level mesothelin expression and a low-level CA125 expression.

Statistical Analysis

We used χ^2 test or Fisher exact test to determine the correlation among mesothelin and CA125 and clinicopathologic data. Survival curves of patients were drawn by the Kaplan-Meier method. Differences in survival curves were analyzed by the log-rank test. All differences were considered significant at $P < 0.05$. All statistical analyses were performed using Statview 5.0 software (SAS Institute Inc, Cary, NC).

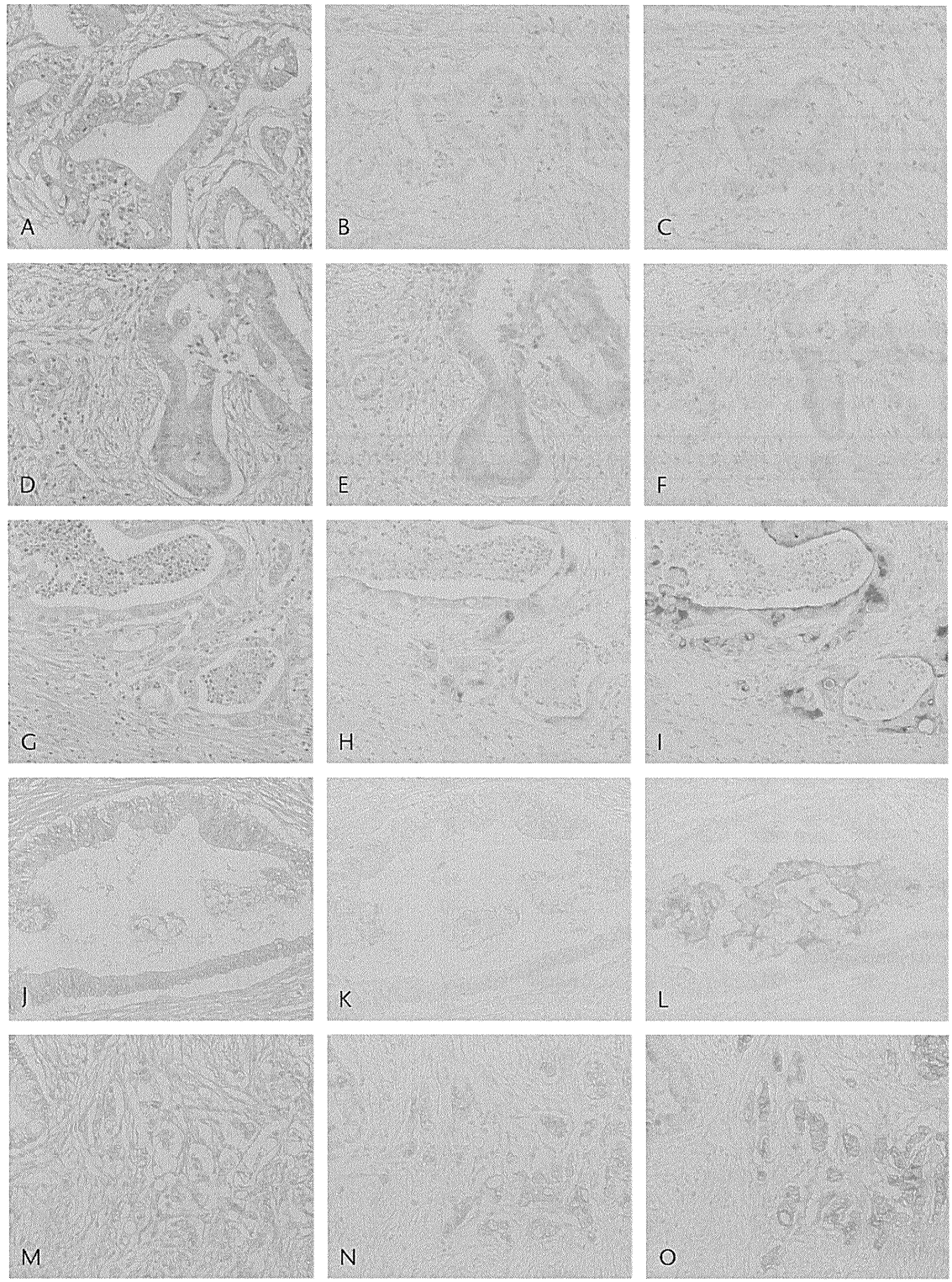

FIGURE 1. Representative cases of pancreatic ductal adenocarcinoma showing scores of 0, 1+, and 2+ for HE, mesothelin, and CA125 expression. Patient 1 was in grade 2 (moderately differentiated ductal adenocarcinoma) (A, HE). There was no mesothelin expression (B), but CA125 (C) reactivity was seen in the cancer cells. Patient 2 was in grade 2 (moderately differentiated ductal adenocarcinoma) (D, HE). Mesothelin (E) and CA125 (F) expressions were detected faintly or barely in the membrane and cytoplasm of cancer cells. Patient 3 was in grade 2 (moderately differentiated ductal adenocarcinoma) (G, HE). Mesothelin (H) and CA125 (I) expressions had moderate to strong staining in cancer cells. Patient 4 was in grade 2 (moderately differentiated ductal adenocarcinoma) (J, HE). Mesothelin expression (K) was weak, whereas CA125 expression (L) was moderate to strong. Patient 5 was in grade 3 (poorly differentiated ductal adenocarcinoma) (M, HE). Mesothelin (N) and CA125 (O) expressions were strong. Immunoperoxidase stain, original magnification×200.

TABLE 2. Mesothelin and CA125 Immunostaining in Pancreatic Ductal Adenocarcinoma

	No. Cases (%)							
	Percentage of Mesothelin-Positive Cells				Percentage of CA125-Positive Cells			
	0	1%–10%	10%–50%	>50%	0	1%–10%	10%–50%	>50%
Staining intensity on tumor cells								
Score 0	9 (13.6)	0 (0)	0 (0)	0 (0)	5 (7.6)	0 (0)	0 (0)	0 (0)
Score 1	0 (0)	17 (25.8)	5 (7.6)	3 (4.5)	0 (0)	6 (9.1)	2 (3.0)	0 (0)
Score 2	0 (0)	3 (4.5)	13 (19.7)	16 (24.2)	0 (0)	4 (6.1)	14 (21.2)	35 (53.0)

RESULTS

Mesothelin and CA125 Expressions in Pancreatic Ductal Adenocarcinoma

In 57 of the 66 pancreatic ductal adenocarcinoma specimens (86.4%), mesothelin was positive in carcinoma cells, whereas 61 (92.4%) of the 66 specimens were positive for CA125 (Table 2).

As shown in Table 3, a high level of mesothelin expression was detected in 35 cases (53.2%). A high mesothelin expression was correlated with a higher histological grade (P = 0.049) and a higher level of blood vessel permeation

TABLE 3. Clinicopathologic Features According to Expression Levels of Mesothelin and CA125

		Mesothelin			CA125			Co-Expression		
Parameter	Total	High Level (n = 35)	Low Level (n = 31)	P	High Level (n = 53)	Low Level (n = 13)	P	Positive (n = 33)	Negative (n = 33)	P
Histological classification										
Grade1/2	55	26	29	**0.049**	42	13	0.10	24	31	**0.044**
Grade3	11	9	2		11	0		9	2	
pT factor										
pT1-2	19	8	11	0.29	16	3	0.74	8	11	0.59
pT3-4	47	27	20		37	10		25	22	
pN factor										
Positive	44	26	18	0.20	37	7	0.33	25	19	0.19
Negative	22	9	13		16	6		8	14	
pStage										
I-II B	58	32	26	0.46	46	12	0.94	30	28	0.71
III-IV	8	3	5		7	1		3	5	
Lymphatic permeation										
Positive	52	26	26	0.38	40	12	0.23	24	28	0.37
Negative	14	9	5		13	1		9	5	
Blood vessel permeation										
Positive	30	23	7	**0.0006**	27	3	0.12	22	8	**0.001**
Negative	36	12	24		26	10		11	25	
Residual tumor										
R0	44	26	18	0.20	37	7	0.33	24	20	0.43
R1	22	9	13		16	6		9	13	
Recurrence										
Yes	53	31	22	0.12	46	7	**0.015**	31	22	0.060
No	13	4	9		7	6		3	10	
Liver metastasis										
Yes	18	13	5	0.095	17	1	0.094	13	5	0.051
No	48	22	26		36	12		20	28	
Local recurrence										
Yes	17	8	9	0.59	14	3	0.80	8	9	0.78
No	49	27	22		39	10		25	24	
Peritoneal metastasis										
Yes	13	6	7	0.76	10	3	0.71	6	7	0.76
No	53	29	24		43	10		26	27	

χ^2/Fisher exact test.
Values in bold are statistically significant.

TABLE 4. Correlation Between Mesothelin and CA125 Expression

	No. Cases (%)		
	CA125 Expression		
	High Level	Low Level	Total
Mesothelin expression			
High level	33 (50.0)	2 (3.0)	35 (53.0)
Low level	20 (30.3)	11 (16.7)	31 (47.0)
Total	53 (80.3)	13 (19.7)	66 (100)

χ^2/Fisher exact test $P = 0.0041$.

($P = 0.0006$). A high CA125 expression was detected in 53 cases (80.3%) and correlated with a higher recurrence rate ($P = 0.015$). Co-expression of mesothelin and CA125 was detected in 33 cases (50.0%) and correlated with a higher histological grade ($P = 0.044$) and a higher level of blood vessel permeation as well ($P = 0.001$). As for the relationship with recurrence, the incidence of co-expression also tended to be associated with a higher recurrence rate, although the difference was not significant ($P = 0.060$).

A high CA125 expression was detected in 33 of the 35 cases expressing a high level of mesothelin, whereas a low level of CA125 expression was detected in only 2. Among the 31 cases expressing a low level of mesothelin, a high level of CA125 expression was detected in 20 cases, whereas a low level of CA125 expression was detected in 11. There was a significant relationship between mesothelin and CA125 expression ($P = 0.0041$) (Table 4).

Patient Outcomes

Fifty-three patients (80.3%) developed recurrent diseases. Common sites of first recurrence were the liver, local region, and peritoneum (Table 3). Within the study period, 51 patients (77.3%) died of the disease.

Clinical Analysis

The incidence of liver metastasis was marginally significant among patients showing co-expression ($P = 0.051$). Figures 2 and 3 show that patients with a high-level expression of either mesothelin or CA125 had a significantly poorer RFS and OS than the group showing low levels of mesothelin and CA125 expression. Moreover, the group showing co-expression had the poorest prognosis.

DISCUSSION

In this study, we present the first clinicopathologic implications of mesothelin and CA125 immunoreactivity in pancreatic ductal adenocarcinoma. We showed that mesothelin and CA125 are co-expression in pancreatic ductal adenocarcinoma and that co-expression of these 2 indicates highly malignant characteristics and predicts a poor prognosis. It is suggested that co-expression plays a significant role in the acquisition of aggressive clinical behavior by pancreatic ductal adenocarcinoma.

A significant finding of this study was that a high level of mesothelin expression was correlated with a higher histological grade and a higher level of blood vessel permeation. Recent studies reported that not only is mesothelin associated with increased cell proliferation and with the migration of pancreatic cancer cells in vitro,[11,30] but also it contributes to tumor progression in vivo.[11] Furthermore, mesothelin inhibits paclitaxel-induced apoptosis through concomitant activation of PI3K (phosphoinositide-3-kinase) signaling in the regulation of Bcl-2 family expression[31] and induces the activation of signal transducer and activator of transcription (Stat) 3, which leads to increased expression of cyclin E and makes pancreatic cancer cells proliferate faster.[30] Our study confirmed the results of recent studies and also provided new evidence that mesothelin expression is associated with the malignant behavior of tumor cells, such as histological grade or vascular invasion.

This study demonstrated that the expression of mesothelin was correlated with that of the CA125 in pancreatic ductal adenocarcinoma. More notably, the group of patients showing co-expression of mesothelin and CA125 had a poorer OS in comparison to that of groups showing a high expression of either mesothelin or CA125 alone. In our clinicopathologic analyses, the co-expression group showed a higher histological grade and a higher level of blood vessel permeation similar to those in the group showing a high level of mesothelin expression and was marginally correlated with recurrence. In ovarian cancer, co-expression of mesothelin and CA125 was found in patients showing an advanced clinical stage and high histological grade.[28] These findings imply that co-expression of

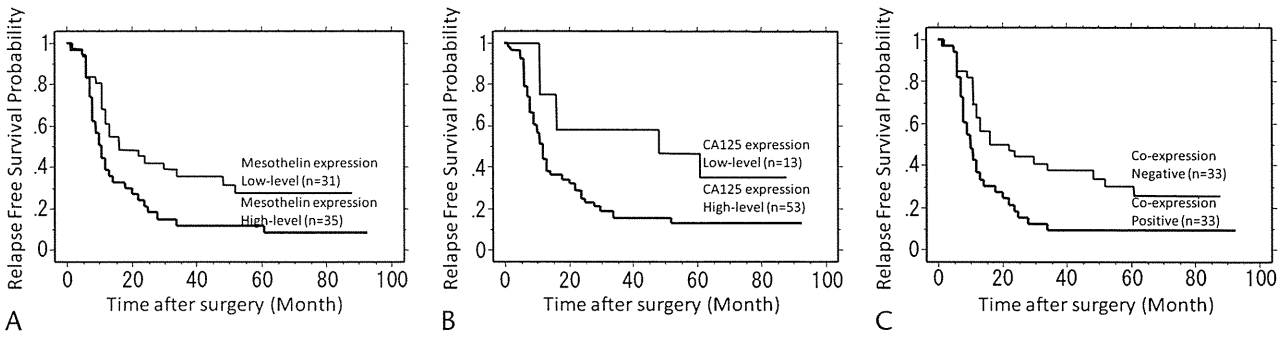

FIGURE 2. Relapse-free survival for patients with pancreatic adenocarcinoma after surgical therapy stratified by the status of mesothelin expression (A), CA125 expression (B), and co-expression (C). A, Curve for patients with tumors showing a high mesothelin expression was significantly worse than that of patients with tumors showing low mesothelin expression (median RFS was 10.0 months for those with high-level mesothelin expression vs 16.0 months for those with low-level mesothelin expression; $P = 0.017$). B, Curve for patients with tumor showing high CA125 expression was significantly worse than that of patients with tumors showing low CA125 expression (median RFS was 12.0 months in high-level CA125 expression vs 40.1 months in low-level CA125 expression; $P = 0.015$). C, Curve for patients with tumor positive for co-expression was significantly worse than that of patients with tumors negative for co-expression (median RFS was 10.0 months for those positive for co-expression vs 16.0 months for those negative for co-expression; $P = 0.0075$).

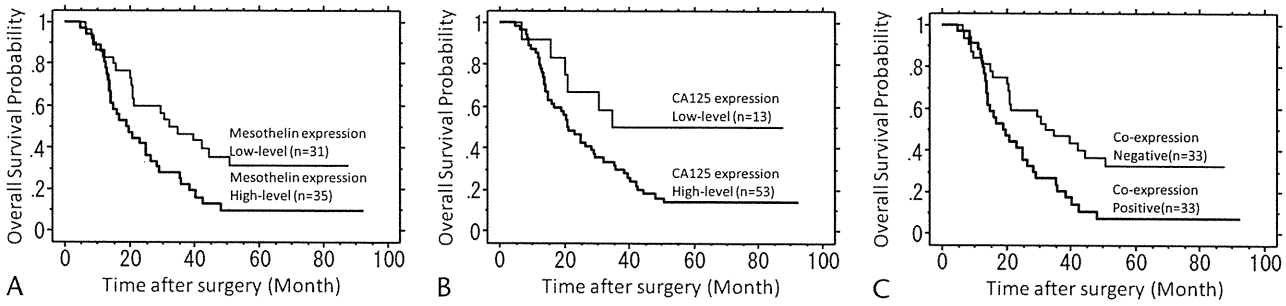

FIGURE 3. Overall survival for patients with pancreatic adenocarcinoma after surgical therapy stratified by the status of mesothelin expression (A), CA125 expression (B), and co-expression (C). A, Curve for patients with tumors showing high mesothelin expression was significantly worse than that of patients with tumors showing low mesothelin expression (median OS was 19.8 months for those showing high mesothelin expression vs 34.8 months for those showing low mesothelin expression; $P = 0.012$). B, Curve for patients with tumors showing high CA125 expression was significantly worse than that of patients with tumors showing low CA125 expression (median OS was 20.9 months in high-level CA125 expression vs 40.1 months in low-level CA125 expression; $P = 0.030$). C, Curve for patients with tumors positive for co-expression was significantly worse than that of patients with tumors negative for co-expression (median OS was 19.0 months in those showing positive co-expression vs 34.8 months in those negative for co-expression; $P = 0.0062$).

mesothelin and CA125 promotes tumor development and metastasis, leading to a poorer patient prognosis, although it remains necessary to clarify the biological function of mesothelin and/or CA125 expression in in vitro and in vivo studies.

Heterotypic adhesion through mesothelin-CA125 high-affinity interaction suggests that mesothelin and/or CA125 expressed on tumor cells can promote intracavitary tumor metastasis by binding to their respective ligands on the mesothelial cells lining the pleura or peritoneum.[26,28] However, this study demonstrated that the incidence of peritoneal metastasis was not correlated with mesothelin or CA125 expression, whereas the incidence of liver metastasis was significantly correlated with co-expression. Such discrepancy might be explained by the fact that liver metastasis usually occurs through vascular invasion because co-expression of mesothelin and CA125 was associated with vessel permeation. In addition, homotypic interaction between co-expression of mesothelin and CA125 on tumor cells might lead to tumor aggregation and potentiate metastasis. In fact, other experiments demonstrated significantly higher homotypic adhesion in cancer cells that coexpressed mesothelin and CA125.[26,32] These findings may indicate that the tumor load at the site of metastasis is increased not only by the uncontrolled expansion of cancer cells, but also by the binding of additional tumor cells derived from the primary or secondary tumor sites.

A better understanding of the mesothelin-CA125 interaction may eventually aid in developing such a therapy. In a previous report, a region (296–359) consisting of 64 amino acids was identified at the N-terminal of cell surface mesothelin as a minimum fragment for complete binding activity to CA125. It was found that substitution of tyrosine 318 with an alanine abolished CA125 binding. Replacement of tryptophan 321 and glutamic acid 324 with alanine partially decreased binding to CA125, whereas mutation of histidine 354 had no effect. These findings indicate that a conformation-sensitive structure of the region (296–359) is required and sufficient for the binding of mesothelin to CA125.[27] In addition, antimesothelin antibody blocks the mesothelin-CA125 interaction on cancer cells.[26–28,33,34] Inhibiting the mesothelin-CA125 interaction could be a useful strategy to prevent tumor metastasis.

There are many published studies demonstrating the prognostic significance of various molecules, for example, epidermal growth factor receptor, c-erbB-2 (HER2), in pancreatic cancer patients.[35,36] Although these molecular prognostic factors are not overwhelming, these specific molecular targeting therapies studies have shown a survival benefit.[37,38] In pancreatic cancer, mesothelin was immunohistochemically expressed in all cases, but was absent in normal pancreas and in chronic pancreatitis.[7,14,15] Therefore, we consider that mesothelin is an attractive candidate for cancer immunotherapy.[11,32,33,39–43]

In conclusion, we have first demonstrated that mesothelin and CA125 were coexpressed in pancreatic ductal adenocarcinoma and that the group showing co-expression had high malignant characteristics and an unfavorable prognosis. This study suggests that the examination of mesothelin and CA125 expression might be useful to predict the potential aggressiveness of pancreatic cancers and that mesothelin and CA125 protein might also serve as a novel molecular target of treatment.

ACKNOWLEDGMENT

The authors thank Dr Yukifumi Kondo for his kindness.

REFERENCES

1. Jemal A, Siegel R, Ward E, et al. Cancer statistics, 2006. *CA Cancer J Clin.* 2006;56:106–130.
2. Matsuno S, Egawa S, Fukuyama S, et al. Pancreatic Cancer Registry in Japan: 20 years of experience. *Pancreas.* 2004;28:219–230.
3. Bramhall SR, Allum WH, Jones AG, et al. Treatment and survival in 13,560 patients with pancreatic cancer, and incidence of the disease, in the West Midlands: an epidemiological study. *Br J Surg.* 1995;82:111–115.
4. Parkin DM, Bray FI, Devesa SS. Cancer burden in the year 2000. The global picture. *Eur J Cancer.* 2001;37(suppl 8):S4–S66.
5. Chang K, Pastan I. Molecular cloning of mesothelin, a differentiation antigen present on mesothelium, mesotheliomas, and ovarian cancers. *Proc Natl Acad Sci U S A.* 1996;93:136–140.
6. Chang K, Pastan I, Willingham MC. Isolation and characterization of a monoclonal antibody, K1, reactive with ovarian cancers and normal mesothelium. *Int J Cancer.* 1992;50:373–381.
7. Argani P, Iacobuzio-Donahue C, Ryu B, et al. Mesothelin is overexpressed in the vast majority of ductal adenocarcinomas of the pancreas: identification of a new pancreatic cancer marker by serial analysis of gene expression (SAGE). *Clin Cancer Res.* 2001;7:3862–3868.
8. Hassan R, Kreitman RJ, Pastan I, et al. Localization of mesothelin in epithelial ovarian cancer. *Appl Immunohistochem Mol Morphol.* 2005;13:243–247.

9. Ordonez NG. Value of mesothelin immunostaining in the diagnosis of mesothelioma. *Mod Pathol*. 2003;16:192–197.
10. Ordonez NG. Application of mesothelin immunostaining in tumor diagnosis. *Am J Surg Pathol*. 2003;27:1418–1428.
11. Li M, Bharadwaj U, Zhang R, et al. Mesothelin is a malignant factor and therapeutic vaccine target for pancreatic cancer. *Mol Cancer Ther*. 2008;7:286–296.
12. Yen MJ, Hsu CY, Mao TL, et al. Diffuse mesothelin expression correlates with prolonged patient survival in ovarian serous carcinoma. *Clin Cancer Res*. 2006;12:827–831.
13. Cheng WF, Huang CY, Chang MC, et al. High mesothelin correlates with chemoresistance and poor survival in epithelial ovarian carcinoma. *Br J Cancer*. 2009;100:1144–1153.
14. Hassan R, Laszik ZG, Lerner M, et al. Mesothelin is overexpressed in pancreaticobiliary adenocarcinomas but not in normal pancreas and chronic pancreatitis. *Am J Clin Pathol*. 2005;124:838–845.
15. Swierczynski SL, Maitra A, Abraham SC, et al. Analysis of novel tumor markers in pancreatic and biliary carcinomas using tissue microarrays. *Hum Pathol*. 2004;35:357–366.
16. Bast RC Jr, Feeney M, Lazarus H, et al. Reactivity of a monoclonal antibody with human ovarian carcinoma. *J Clin Invest*. 1981;68:1331–1337.
17. Kabawat SE, Bast RC Jr, Bhan AK, et al. Tissue distribution of a coelomic-epithelium-related antigen recognized by the monoclonal antibody OC125. *Int J Gynecol Pathol*. 1983;2:275–285.
18. Bateman AC, al-Talib RK, Newman T, et al. Immunohistochemical phenotype of malignant mesothelioma: predictive value of CA125 and HBME-1 expression. *Histopathology*. 1997;30:49–56.
19. Fuith LC, Daxenbichler G, Dapunt O. CA 125 in the serum and tissue of patients with gynecological disease. *Arch Gynecol Obstet*. 1987;241:157–164.
20. Kushitani K, Takeshima Y, Amatya VJ, et al. Immunohistochemical marker panels for distinguishing between epithelioid mesothelioma and lung adenocarcinoma. *Pathol Int*. 2007;57:190–199.
21. Baratti D, Kusamura S, Martinetti A, et al. Circulating CA125 in patients with peritoneal mesothelioma treated with cytoreductive surgery and intraperitoneal hyperthermic perfusion. *Ann Surg Oncol*. 2007;14:500–508.
22. Bast RC Jr, Badgwell D, Lu Z, et al. New tumor markers: CA125 and beyond. *Int J Gynecol Cancer*. 2005;15(suppl 3):274–281.
23. Simsek H, Kadayifci A, Okan E. Importance of serum CA 125 levels in malignant peritoneal mesothelioma. *Tumour Biol*. 1996;17:1–4.
24. O'Brien TJ, Beard JB, Underwood LJ, et al. The CA 125 gene: a newly discovered extension of the glycosylated N-terminal domain doubles the size of this extracellular superstructure. *Tumour Biol*. 2002;23:154–169.
25. Yin BW, Lloyd KO. Molecular cloning of the CA125 ovarian cancer antigen: identification as a new mucin, MUC16. *J Biol Chem*. 2001;276:27371–27375.
26. Gubbels JA, Belisle J, Onda M, et al. Mesothelin-MUC16 binding is a high affinity, N-glycan dependent interaction that facilitates peritoneal metastasis of ovarian tumors. *Mol Cancer*. 2006;5:50.
27. Kaneko O, Gong L, Zhang J, et al. A binding domain on mesothelin for CA125/MUC16. *J Biol Chem*. 2009;284:3739–3749.
28. Rump A, Morikawa Y, Tanaka M, et al. Binding of ovarian cancer antigen CA125/MUC16 to mesothelin mediates cell adhesion. *J Biol Chem*. 2004;279:9190–9198.
29. Sobin LH, Wittekind C. *TNM Classification of Malignant Tumors*. 6th ed. New York: Wiley-Liss; 2002.
30. Bharadwaj U, Li M, Chen C, et al. Mesothelin-induced pancreatic cancer cell proliferation involves alteration of cyclin E via activation of signal transducer and activator of transcription protein 3. *Mol Cancer Res*. 2008;6:1755–1765.
31. Chang MC, Chen CA, Hsieh CY, et al. Mesothelin inhibits paclitaxel-induced apoptosis through the PI3K pathway. *Biochem J*. 2009;424:449–458.
32. Hassan R, Schweizer C, Lu KF, et al. Inhibition of mesothelin–CA-125 interaction in patients with mesothelioma by the anti-mesothelin monoclonal antibody MORAb-009: implications for cancer therapy. *Lung Cancer*. 2010;68:455–459.
33. Hassan R, Ebel W, Routhier EL, et al. Preclinical evaluation of MORAb-009, a chimeric antibody targeting tumor-associated mesothelin. *Cancer Immun*. 2007;7:20.
34. Ho M, Feng M, Fisher RJ, et al. A novel high-affinity human monoclonal antibody to mesothelin. *Int J Cancer*. 2011;128:2020–2030.
35. Ueda S, Ogata S, Tsuda H, et al. The correlation between cytoplasmic overexpression of epidermal growth factor receptor and tumor aggressiveness: poor prognosis in patients with pancreatic ductal adenocarcinoma. *Pancreas*. 2004;29:e1–e8.
36. Saxby AJ, Nielsen A, Scarlett CJ, et al. Assessment of HER-2 status in pancreatic adenocarcinoma: correlation of immunohistochemistry, quantitative real-time RT-PCR, and FISH with aneuploidy and survival. *Am J Surg Pathol*. 2005;29:1125–1134.
37. Kindler HL, Friberg G, Singh DA, et al. Phase II trial of bevacizumab plus gemcitabine in patients with advanced pancreatic cancer. *J Clin Oncol*. 2005;23:8033–8040.
38. Moore MJ, Goldstein D, Hamm J, et al. Erlotinib plus gemcitabine compared with gemcitabine alone in patients with advanced pancreatic cancer: a phase III trial of the National Cancer Institute of Canada Clinical Trials Group. *J Clin Oncol*. 2007;25:1960–1966.
39. Hassan R, Bera T, Pastan I. Mesothelin: a new target for immunotherapy. *Clin Cancer Res*. 2004;10:3937–3942.
40. Hassan R, Broaddus VC, Wilson S, et al. Anti-mesothelin immunotoxin SS1P in combination with gemcitabine results in increased activity against mesothelin-expressing tumor xenografts. *Clin Cancer Res*. 2007;13:7166–7171.
41. Hassan R, Bullock S, Premkumar A, et al. Phase I study of SS1P, a recombinant anti-mesothelin immunotoxin given as a bolus I.V. infusion to patients with mesothelin-expressing mesothelioma, ovarian, and pancreatic cancers. *Clin Cancer Res*. 2007;13:5144–5149.
42. Hassan R, Ho M. Mesothelin targeted cancer immunotherapy. *Eur J Cancer*. 2008;44:46–53.
43. Inami K, Abe M, Takeda K, et al. Antitumor activity of anti-C-ERC/mesothelin monoclonal antibody in vivo. *Cancer Sci*. 2010;101:969–974.

Inflamm. Res. (2011) 60:879–888
DOI 10.1007/s00011-011-0348-z

Inflammation Research

ORIGINAL RESEARCH PAPER

Inhibition of macrophage activation and suppression of graft rejection by DTCM-glutarimide, a novel piperidine derived from the antibiotic 9-methylstreptimidone

Masatoshi Takeiri · Miyuki Tachibana · Ayumi Kaneda · Ayumi Ito · Yuichi Ishikawa · Shigeru Nishiyama · Ryoichi Goto · Kenichiro Yamashita · Susumu Shibasaki · Gentaro Hirokata · Michitaka Ozaki · Satoru Todo · Kazuo Umezawa

Received: 14 November 2010 / Revised: 15 April 2011 / Accepted: 13 May 2011 / Published online: 28 May 2011

Abstract
Objective We have previously synthesized a novel piperidine compound, 3-[(dodecylthiocarbonyl)methyl] glutarimide (DTCM-glutarimide), that inhibits LPS-induced NO production, and in the present research we studied further the anti-inflammatory activity of DTCM-glutarimide in a macrophage cell line and in mice bearing transplanted hearts.
Materials and methods Mouse macrophage-like RAW264.7 cells were employed for the evaluation of cellular inflammatory activity. DTCM-glutarimide was synthesized in our laboratory. The AP-1 activity was measured by nuclear translocation and phosphorylation. For the heart transplantation experiment, male C57BL/6 (H-2b) and BALB/c (H-2d) mice were used as donor and recipient, respectively. DTCM-glutarimide was administered intraperitoneally.
Results DTCM-glutarimide inhibited the LPS-induced expression of iNOS and COX-2 in macrophages; but, unexpectedly, it did not inhibit LPS-induced NF-κB activation. Instead, it inhibited the nuclear translocation of both c-Jun and c-Fos. It also inhibited LPS-induced c-Jun phosphorylation. Moreover, it inhibited the mixed lymphocyte reaction in primary cultures of mouse spleen cells; and furthermore, in mice it prolonged the graft survival in heart transplantation experiments.
Conclusion The novel piperidine compound, DTCM-glutarimide, was found to be a new inhibitor of macrophage activation, inhibiting AP-1 activity. It also inhibited graft rejection in mice, and thus may be a candidate for an anti-inflammatory agent.

Keywords DTCM-glutarimide · LPS · AP-1 · Mixed lymphocyte reaction · Heart transplantation

Responsible Editor: Graham Wallace.

M. Takeiri · M. Tachibana · A. Kaneda · A. Ito · Y. Ishikawa · S. Nishiyama · K. Umezawa (✉)
Center for Chemical Biology, School of Fundamental Science and Technology, Faculty of Science and Technology, Keio University, 3-14-1 Hiyoshi, Kohoku-ku, Yokohama 223-0061, Japan
e-mail: umezawa@applc.keio.ac.jp

R. Goto · K. Yamashita · S. Shibasaki · G. Hirokata · M. Ozaki · S. Todo
Department of Surgery, Hokkaido University School of Medicine, Sapporo 060-8683, Japan

Introduction

Microbial and plant-derived bioactive metabolites are a treasure-trove of organic compounds having various structures and biological activities. Molecular designing of these bioactive metabolites often provides further active and useful compounds. We have previously designed dehydroxymethylepoxyquinomicin (DHMEQ) based on the structure of epoxyquinomicins, which are weak antibiotics isolated from *Amicolatopsis* [1, 2]. DHMEQ inhibits NF-κB by direct binding to NF-κB components including p65, p50, RelB, and cRel [3], and it shows potent anti-inflammatory and anticancer effects in animal experiments [4–6]. It also prolongs the graft survival in mouse heart transplantation experiments [7]. Since DHMEQ was effective in suppression of many disease models, further screening for NF-κB inhibitors was carried out in which NF-κB activity was monitored in terms of lipopolysaccharide (LPS)-induced NO production in macrophages. Thereby, we isolated 9-methylstreptimidone, a known piperidine compound (Fig. 1), from *Streptomyces* and

found this NF-κB inhibitor selectively induces apoptosis in adult T-cell leukemia cells in which NF-κB is excessively activated [8]. Since the production of 9-methylstreptimidone by the producing organism is poor, we synthesized a number of its derivatives. Among them, we found 3-[(dodecylthiocarbonyl)methyl]glutarimide (DTCM-glutarimide, Fig. 1) to inhibit LPS-induced NO production strongly in mouse macrophage RAW264.7 cells [9].

In the present research we studied further the anti-inflammatory activity of DTCM-glutarimide in a macrophage cell line. This analog inhibited the expression of iNOS and COX-2, possibly due to the inhibition of AP-1 activation. It also showed anti-inflammatory activity in a transplantation experiment.

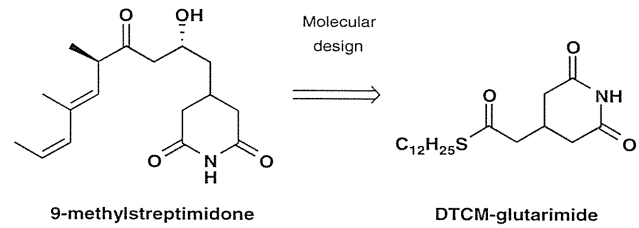

Fig. 1 Structures of 9-methylstreptimidone and DTCM-glutarimide

Materials and methods

Materials

DTCM-glutarimide (3-[(dodecylthiocarbonyl)methyl]glutarimide) was synthesized by us as described earlier [9]. Mouse monoclonal anti-COX-2 antibody was purchased from BD Bioscience Pharmingen, Franklin Lakes, NJ, USA. Mouse monoclonal anti-NOS2, anti-ERK1, and anti-p65 NF-κB and rabbit polyclonal anti-p38, anti-JNK, and anti-c-Fos antibodies were obtained from Santa Cruz Biotechnology, CA, USA. Rabbit polyclonal anti-phospho-p38, anti-phospho-p44/42 MAP kinase, anti-phospho-JNK, and anti-lamin A/C, as well as rabbit monoclonal anti-c-Jun and anti-phospho-c-Jun antibodies, were purchased from Cell Signaling Technology, Beverly, MO, USA. Anti-rabbit-IgG antibody derived from goat and anti-mouse-IgG antibody derived from sheep were purchased from GE Healthcare, Little Chalfont, UK. Anti-α-tubulin antibody was purchased from Sigma-Aldrich, St. Louis, MO, USA.

Cell culture

Mouse macrophage RAW264.7 cells were grown in Dulbecco's modified Eagle's medium (DMEM; Nissui, Tokyo, Japan) supplemented with 10% fetal bovine serum (JRH Biosciences, Lenexa, KS, USA), 200 μg/ml kanamycin (Sigma, St. Louis, MO, USA), 100 units/ml penicillin G (Sigma), 600 μg/ml L-glutamine (Sigma), and 2.25 g/L $NaHCO_3$ at 37°C under 5% CO_2 plus air.

NO production assay

Cells in complete medium (1×10^5 cells/ml) were seeded in a 96-well plate (Corning Inc., Corning, NY, USA), with each well receiving 100 μl of the cell suspension. On the next day, the cells were treated with DTCM-glutarimide for 2 h and then stimulated with 3 μg/ml LPS for 20 h. Then 100 μl Griess reagent solution was added to each well [21]. The concentration of NO was obtained by measuring the absorbance at 570 nm with a microplate reader.

MTT assay

Cells in complete medium (1×10^5 cells/ml) were seeded in a 96-well plate, with each well receiving 100 μl of the cell suspension. On the next day, the cells were treated with DTCM-glutarimide for 2 h and then stimulated with 3 μg/ml LPS for 20 h. Then, 10 μl of MTT (3-[4,5-dimethylthiazol-2–yl]-2,5-diphenyltetrazoliumbromide) solution was added to each well, and the cells were incubated for 4 h at 37°C under 5% CO_2 plus air. Subsequently, the culture supernatant was replaced with 100 μl DMSO to dissolve the formazan crystals made from MTT by the enzymatic action of succinic dehydrogenase in the mitochondria of live cells. The absorbance at 570 nm was measured with a microplate reader.

Western blotting

Cells in complete medium (1×10^5 or 3×10^5 cells/ml) were seeded into 60-mm dishes (Corning). On the next day, the cells were treated with DTCM-glutarimide for 2 h and then stimulated with 3 μg/ml LPS for the desired times. Then the cells were lysed with lysis buffer (20 mM Tris [pH 8.0], 150 mM NaCl, 2 mM EDTA, 100 mM NaF, 400 μM Na_3VO_4, 1% Nonidet P-40, 1 μg/ml leupeptin, 1 μg/ml aprotinin, and 1 mM PMSF). Total cell extracts or nuclear extracts (about 10–30 μg of protein) were boiled in Laemmli loading buffer and subjected to SDS-polyacrylamide gel electrophoresis. Proteins were transferred at 200 mA for 1 h onto Hybond-P membranes (GE Healthcare, Little Chalfont, UK). The membranes were incubated for 30 min at room temperature (RT) for blocking in Tris-buffered saline with Tween 20 (TBST), composed of 10 mM Tris–HCl, pH 8.0, containing 150 mM NaCl, 0.1% Tween 20 (v/v), and 5% (w/v) nonfat dry milk. After

having been washed for 1 h in TBST, the membrane was incubated for 1 h at RT in a 1:3,000 dilution of a primary antibody in TBST. After a 1 h wash in TBST, the membrane was next incubated for 1 h at RT with anti-IgG rabbit or anti-IgG mouse antibody (diluted at 1:3,000 in TBST) linked to horseradish peroxidase. After having been washed for 1 h in TBST, immunoreactive proteins were visualized by use of an ECL detection system, Immobilon Western (Millipore, Billerica, MA, USA). Exposure to RX-U films (Fuji Film, Kanagawa, Japan) was carried out for 10 s to 10 min.

RT-PCR

Cells in complete medium (1×10^5 cells/ml) were seeded into 60-mm dishes (Corning). On the next day, the cells were treated with DTCM-glutarimide for 2 h and then stimulated with 3 μg/ml LPS for the desired times. Total cellular mRNAs were extracted from cells using Trizol reagent (Invitrogen, Carlsbad, CA, USA), then 1 μg of mRNA was converted to cDNA using High-Capacity cDNA Reverse Transcription Kits (Life Technology, Carlsbad, CA, USA), and 2 μl of the cDNA mixture was used for enzymatic amplification using TaKaRa Taq™ (Takara Bio, Shiga, Japan). The primer sequences were 5′-TTTGACCAGAGGACCCAGAG and 5′-ATGGCCG ACCTGATGTTGCC (for iNOS), 5′-AGAAGGAAATGG CTGCAGAA and 5′-GCTCGGCTTCCAGTATTGAG (for COX-2), 5′-CTTCGAGCACGAGATGGCCA and 5′-CC AGACAGCACTGTGTTGGC (for β-actin).

Enzyme-linked immunosorbent assay

Cells in complete medium (4×10^5 cells/ml) were seeded into a 48-well plate (Corning), with each well receiving 500 μl of the cell suspension. On the next day, the cells were treated with DTCM-glutarimide for 2 h and then stimulated with 3 μg/ml LPS for 20 h. The cell-free medium was collected into a 1.5 ml tube and stored at −80°C prior to the assay. The concentration of IL-6 was quantified by using a commercially available sandwich-type enzyme-linked immunosorbent assay (ELISA) kit specific for murine IL-6 (Techne, Minneapolis, MN, USA). After the wells had been coated with the specific antibodies, 2 h later they were washed with wash buffer; then the thawed medium was added to the assay wells. Next, the appropriate horseradish peroxidase-conjugated polyclonal antibody against IL-6 was added, and the plate was incubated for 2 h at RT. After the wells had been washed with Ca^{2+}, Mg^{2+}-free PBS (PBS^-)—Tween, the substrate solution was added to the wells. The color reaction was stopped by the addition of sulfuric acid, and the intensity was expressed by absorbance (A450–A570) read with a microplate reader. The standard curve for IL-6 protein was prepared as indicated by the manufacturer, and the protein level in the sample was calculated from this standard curve.

Immunofluorescence

Cells in complete medium (1×10^6 cells/ml) were seeded onto glass coverslips in a 12-well plate (Corning). On the next day, the cells were treated with DTCM-glutarimide for 2 h and then stimulated with 3 μg/ml LPS for 30 min. Next, the cells were fixed for 10 min with 3% paraformaldehyde in PBS^-, washed 2 times with PBS^-, and permeabilized for 5 min with 1% Triton X in PBS^-. After having been washed again 2 times with PBS^-, the cells were incubated with 10% normal blocking serum in 500 μl of PBS^- for 20 min at RT and washed three times with PBS^-. Then, they were stained with anti-p65, anti-c-Fos antibody (Santa Cruz Biotechnology, California, USA) or anti-c-Jun antibody (Cell Signaling Technology, Beverly, MA, USA) for 45 min at RT, washed 3 times with PBS^-, and stained with anti-rabbit-FITC secondary antibody (Molecular Probes, Reiden, The Netherlands) for 1 h at RT. After three final washings with PBS^-, the cells were photographed through B2 and UV filters at a magnification of 400× with a camera attached to a confocal microscope.

Nuclear protein extraction

Nuclear extracts were prepared according to the method described before [10]. Cells (3×10^5 cells/ml) were grown in 60-mm dishes (Corning) and incubated with the desired chemicals. They were then harvested and washed with phosphate-buffered saline (PBS), suspended in 400 μl of buffer A (10 mM HEPES [pH 7.8], 10 mM KCl, 2 mM $MgCl_2$, 0.1 mM EDTA, 1 mM DTT, 0.1 mM PMSF), and incubated on ice for 15 min. Nuclei were pelleted by centrifugation for 5 min at 14,000 rpm, resuspended in 20–40 μl of buffer C (50 mM HEPES [pH 7.8], 50 mM KCl, 300 mM NaCl, 0.1 mM EDTA, 1 mM DTT, 0.1 mM PMSF, 25% glycerol [v/v]), incubated on ice for 20 min, and centrifuged for 5 min at 14,000 rpm at 4°C. The supernatant was used as the nuclear extract.

Electrophoresis mobility shift assay (EMSA)

The binding reaction mixture contained nuclear extract (5 μg of protein), 2 μg poly (dI-dC), and 10,000 cpm of a ^{32}P-labeled probe (oligonucleotide containing NF-κB binding site) in binding buffer (75 mM NaCl, 1.5 mM EDTA, 1.5 mM DTT, 7.5% glycerol, 1.5% NP-40, 15 mM Tris–HCl; pH 7.0). Samples were incubated for 20 min at RT in this mixture. DNA/protein complexes were separated

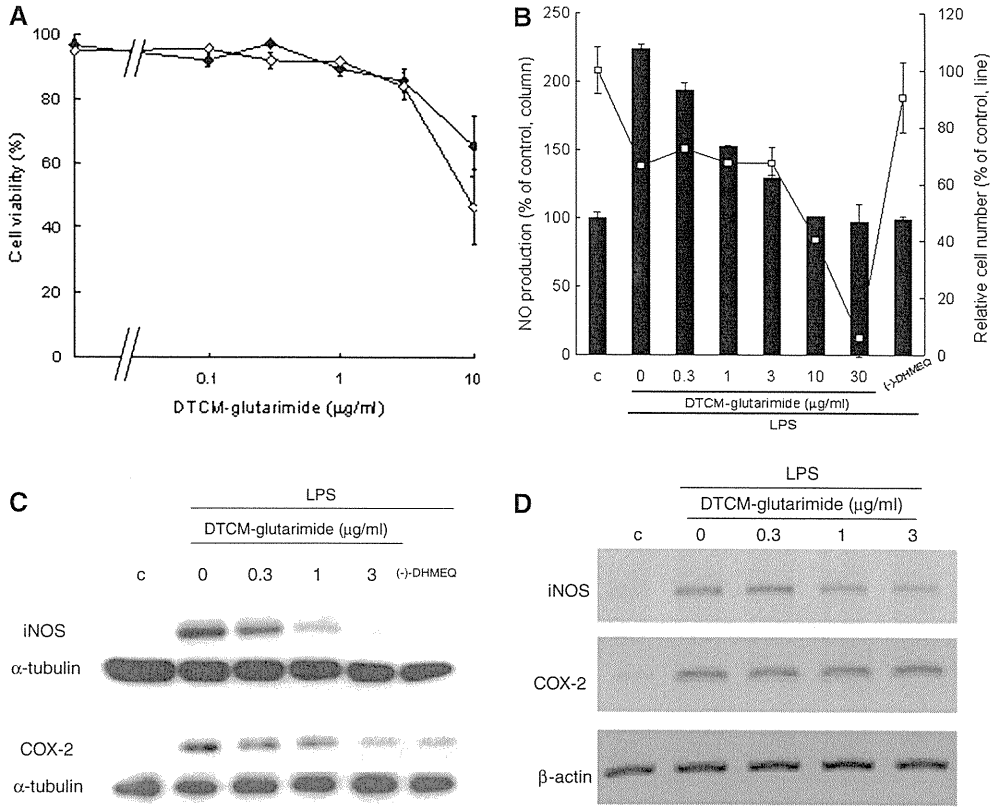

Fig. 2 Inhibition of LPS-induced NO production by DTCM-glutarimide. **a** Effect on cell viability. RAW264.7 cells were incubated with DTCM-glutarimide for 24 h (*black circles*) or 48 h (*white circles*). Cell viability was assessed by performing the trypan blue dye exclusion. The data are the mean ± SD of four determinations. The solvent control did not affect the cellular viability. **b** Inhibition of LPS-induced NO production. The cells were treated with DTCM-glutarimide or 10 μg/ml (−)-DHMEQ for 2 h, then stimulated with 3 μg/ml LPS and co-incubated with each drug for 20 h. NO production was measured by performing the Griess assay. The cell viability in the presence of LPS was measured by use of the MTT assay. The data are the mean ± SD of 3 determinations. **c** Inhibition by DTCM-glutarimide of LPS-induced expression of iNOS and COX-2. **d** Effect of DTCM-glutariomide on iNOS and COX-2 mRNA expression. The cells were treated with DTCM-glutarimide for 2 h, then stimulated with 3 μg/ml LPS and co-incubated with drug for 20 h

from free DNA on 4% native polyacrylamide gel in 0.25 mM TBE buffer. The DNA probes used for NF-κB binding were purchased from Promega (Madison, WI, USA). The following sequences were used as the NF-κB binding site: 5′-AGT TGA GGG GAC TTT CCC AGG C and 5′-GCC TGG GAA AGT CCC CTC AAC T. These oligonucleotides were labeled with [γ-^{32}P]-ATP (3,000 Ci/mmol; GE Healthcare, Little Chalfont, UK) by use of T4 polynucleotide kinase (Takara, Shiga, Japan), and purified by passage through a Nick column (GE Healthcare, Little Chalfont, UK).

In vitro kinase assay

Recombinant human JNK1α1 (20 ng; Millipore, Billerica, MA, USA) was incubated with 10 μCi [γ-32P]-ATP (3000 Ci/mmol; GE Healthcare, Little Chalfont, UK), 50 μM ATP (Sigma, St. Louis, MO, USA), and 2 μg recombinant human c-Jun (Sigma) in 30 μl of kinase buffer (20 mM HEPES, 10 mM MgCl2, 1 mM DTT, 1% Phosphatase Inhibitor Cocktail 2 [Sigma]). Reactions were incubated at 30°C for 1 h and terminated by the addition of Laemmli loading buffer. Proteins were separated by 10% SDS-PAGE, and phosphorylation was visualized by autoradiography.

Lymphocyte stimulation and mixed lymphocyte reaction assay

Purified C57BL/6 mouse-T cells (5×10^5/well) were stimulated with anti-CD28 (1 μg/ml) and plate pre-coated anti-CD3 (10 μg/ml) monoclonal antibodies, and were cultured in 96-well flat-bottomed plates (Costar, NY, USA). For mixed lymphocyte cultures (MLCs), irradiated (30 Gy, ^{137}Cs) BALB/c mouse splenocytes (5×10^5/well) were co-cultured with C57BL/6 mouse splenocytes (5×10^5/well) in 96-well round-bottomed plates (Corning). The plates were incubated at 37°C under 5% CO_2 plus

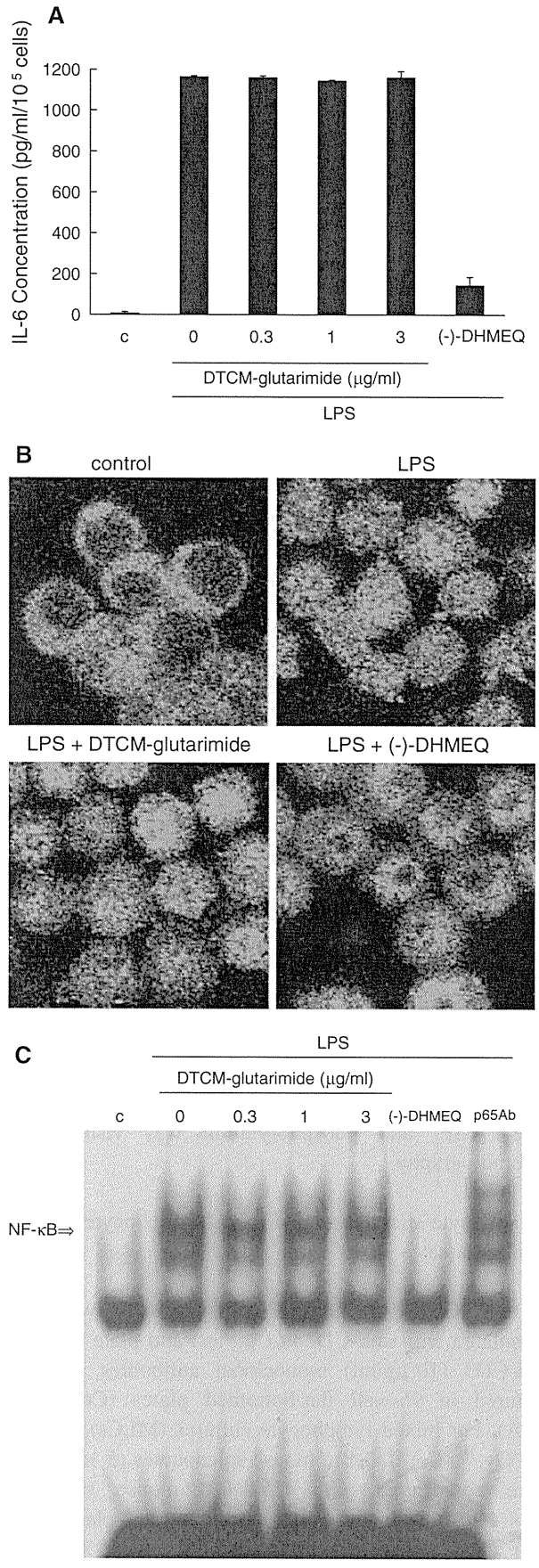

Fig. 3 Lack of NF-κB inhibition by DTCM-glutarimide. **a** Effect on LPS-induced IL-6 secretion. RAW264.7 cells were pretreated with DTCM-glutarimide or 10 μg/ml (−)-DHMEQ, and then stimulated with 3 μg/ml LPS and co-incubated with each drug for 20 h. IL-6 secretion was assessed by performing an ELISA. The data are the mean ± SD of three determinations. **b** Effect on LPS-induced NF-κB nuclear translocation. The cells were pretreated with 3 μg/ml DTCM-glutarimide or (−)-DHMEQ, and stimulated with LPS and co-incubated with each drug for 30 min. Then they were stained with p65 antibody, and analyzed by fluorescence microscopy. **c** Effect on LPS-induced NF-κB activation assessed by use of the EMSA. Nuclear extracts were prepared, and then mixed and incubated with a ^{32}P-labeled NF-κB probe for 20 min in the presence or absence of antibody against p65

air. Cells were pulsed with ^{3}H-thymidine (1 μCi/well) for 16 h before culture termination, and ^{3}H-thymidine incorporation was measured by using a β-counter (PerkinElmer, Boston, MA, USA).

Cardiac transplantation and treatment protocol

Male C57BL/6 (H-2^{b}) and BALB/c (H-2^{d}) mice (SLC Inc., Shizuoka, Japan) was used as donor and recipient, respectively. Heterotopic heart transplantation was performed according to the method previously described by Corry et al. [11]. Cardiac recipients were treated with either DTCM-glutarimide (10–60 mg/kg/day) or control vehicle (0.5% CMC). These agents were administered intraperitoneally, from day 0 to day 13. Graft beating was monitored by daily palpation, and was scored +1 to +4 based on the strength of graft contraction. Rejection was defined as cessation of beating, which was confirmed by direct inspection followed by histopathologic examination. Graft survival time was plotted by the Kaplan–Meier method, and a log-rank test was applied for comparison. A P value of less than 0.05 was considered statistically significant.

The animal experiments were approved by the Institutional Animal Care and Use Committee, and were conducted under the guidelines of our animal care policy.

Histology and immunohistochemistry

Cardiac graft was excised at the time of animal death. Tissues were fixed in 10% formalin, embedded in paraffin, and stained with hematoxylin and eosin (H&E). Graft samples were also embedded in an optimal cutting temperature compound, frozen in liquid nitrogen, and stored at −80°C. Frozen sections were stained with anti-CD4 (GK1.5: Santa Cruz Biotechnology, Santa Cruz, CA) and CD8 (KT15: AbD Serotec, Oxford, UK) Abs using the avidin–biotin complex method as previously described [12]. Positive cells were counted in three different high power fields (HPFs; magnification ×400).

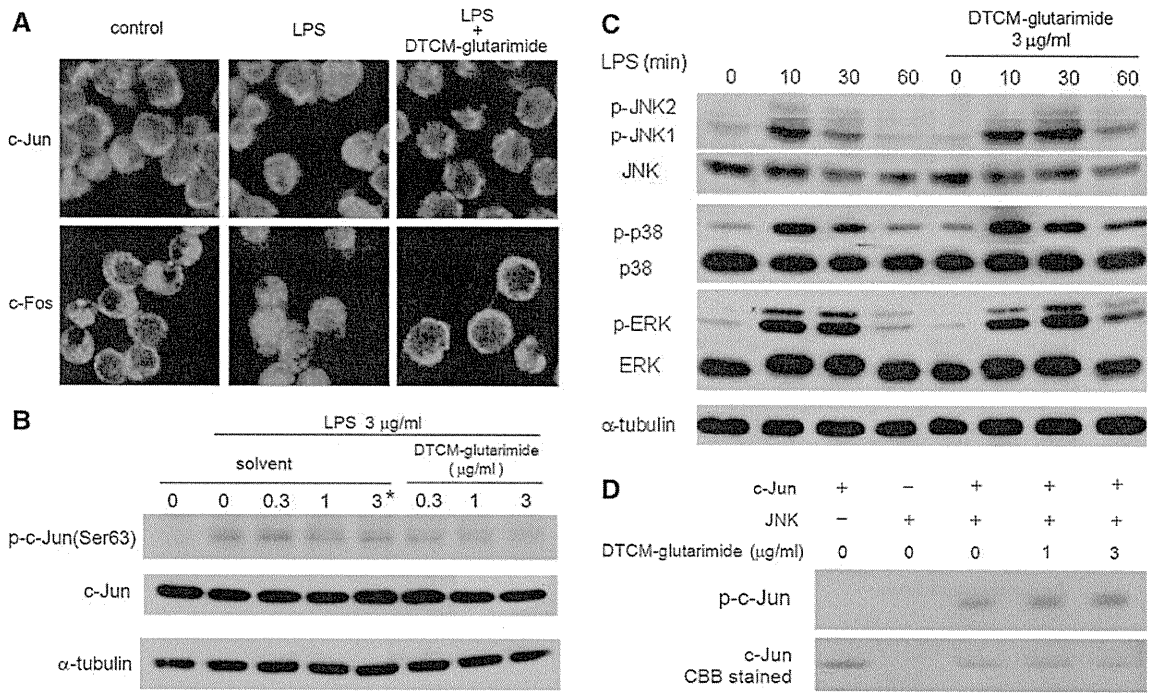

Fig. 4 Inhibition of LPS-induced AP-1 activation by DTCM-glutarimide. **a** Inhibition of LPS-induced nuclear translocation of c-Jun and c-Fos. Cells were pretreated or not with 3 μg/ml DTCM-glutarimide, stimulated or not with LPS and co-incubated with each drug for 30 min, and then analyzed by fluorescence microscopy. **b** Inhibition of c-Jun phosphorylation. Total cell extracts or nuclear extracts were prepared for Western blotting analysis. The proteins were immunoblotted with the indicated antibodies. The asterisk indicates the effect of DMSO alone at 0.3, 1, and 3 μg/ml DTCM-glutarimide; 0.3 (3 μl/ml), 1 (10 μl/ml), and 3 (30 μl/ml). **c** Effect on LPS-induced activation of MAPKs. Activation of MAPK proteins was measured in terms of the phosphorylation of each protein, as assessed by Western blot analysis. **d** Effect on JNK activity in vitro. Recombinant JNK1 and c-Jun were incubated with radioactive ATP for 1 h. Proteins were separated by SDS-PAGE, and phosphorylated c-Jun was visualized by autoradiography

Results

Inhibition of LPS-induced NO production and iNOS expression by DTCM-glutarimide

As shown in Fig. 2a, DTCM-glutarimide did not decrease the viability of RAW264.7 cells after 24 or 48 h when used at concentrations below 3 μg/ml. DTCM-glutarimide at 1–3 μg/ml clearly inhibited the LPS-induced NO production without any toxicity, just as did the NF-κB inhibitor (−)-DHMEQ [1–3], as shown in Fig. 2b. NO is produced mainly by inducible NO synthase (iNOS). LPS induced iNOS expression, which was strongly inhibited by DTCM-glutarimide (Fig. 2c). As the mechanism of inhibition, DTCM-glutarimide inhibited the iNOS mRNA expression (Fig. 2d). The analog also inhibited LPS-induced cyclooxygenase (COX)-2 protein expression weakly, but it did not inhibit the mRNA expression.

Lack of NF-κB inhibition by DTCM-glutarimide

IL-6 secretion is highly dependent on NF-κB, especially in RAW264.7 cells. Unexpectedly, DTCM-glutarimide did not inhibit LPS-induced IL-6 secretion at all, unlike (−)-DHMEQ (Fig. 3a). Then we studied the inhibition of NF-κB and found that its nuclear translocation was not inhibited by DTCM-glutarimide, as shown in Fig. 3b. Furthermore, the LPS-induced activation of NF-κB detected by EMSA was not inhibited by the analog (Fig. 3c).

Inhibition of LPS-induced AP-1 activation by DTCM-glutarimide

iNOS expression is positively regulated by transcription factors including NF-κB and also AP-1 [13]. LPS induced the nuclear translocation of AP-1 components c-Jun and c-Fos in RAW264.7 cells, and DTCM-glutarimide at 3 μg/ml clearly inhibited this translocation of both of them in the immunofluorescence assay, as shown in Fig. 4a. The phosphorylation of AP-1 components is known to occur before their nuclear translocation. By Western blot analysis, we found that DTCM-glutarimide inhibited the phosphorylation of c-Jun (Fig. 4b). In Fig. 4b, we confirmed the effect of solvent alone to exclude the solvent effects. In other experiments, we used DMSO at lower